www.nature.com/aps

Acta Pharmacologica Sinica

ARTICLE

Enhanced AMPAR-dependent synaptic transmission by S-nitrosylation in the vmPFC contributes to chronic inflammatory pain-induced persistent anxiety in mice

Zhi-jin Chen[1], Chun-wan Su[1], Shuai Xiong[1], Ting Li[1], Hai-ying Liang[1,2], Yu-hui Lin[1], Lei Chang[1], Hai-yin Wu[1,3], Fei Li[4], Dong-ya Zhu[1,3] and Chun-xia Luo[1,3]

Chronic pain patients often have anxiety disorders, and some of them suffer from anxiety even after analgesic administration. In this study, we investigated the role of AMPAR-mediated synaptic transmission in the ventromedial prefrontal cortex (vmPFC) in chronic pain-induced persistent anxiety in mice and explored potential drug targets. Chronic inflammatory pain was induced in mice by bilateral injection of complete Freund's adjuvant (CFA) into the planta of the hind paws; anxiety-like behaviours were assessed with behavioural tests; S-nitrosylation and AMPAR-mediated synaptic transmission were examined using biochemical assays and electrophysiological recordings, respectively. We found that CFA induced persistent upregulation of AMPAR membrane expression and function in the vmPFC of anxious mice but not in the vmPFC of non-anxious mice. The anxious mice exhibited higher S-nitrosylation of stargazin (an AMPAR-interacting protein) in the vmPFC. Inhibition of S-nitrosylation by bilaterally infusing an exogenous stargazin (C302S) mutant into the vmPFC rescued the surface expression of GluA1 and AMPAR-mediated synaptic transmission as well as the anxiety-like behaviours in CFA-injected mice, even after ibuprofen treatment. Moreover, administration of ZL006, a small molecular inhibitor disrupting the interaction of nNOS and PSD-95 (20 mg·kg^{-1}·d^{-1}, for 5 days, i.p.), significantly reduced nitric oxide production and S-nitrosylation of AMPAR-interacting proteins in the vmPFC, resulting in anxiolytic-like effects in anxious mice after ibuprofen treatment. We conclude that S-nitrosylation is necessary for AMPAR trafficking and function in the vmPFC under chronic inflammatory pain-induced persistent anxiety conditions, and nNOS-PSD-95 inhibitors could be potential anxiolytics specific for chronic inflammatory pain-induced persistent anxiety after analgesic treatment.

Keywords: chronic pain; anxiety; vmPFC; AMPAR trafficking; S-nitrosylation; stargazin

Acta Pharmacologica Sinica (2023) 44:954–968; https://doi.org/10.1038/s41401-022-01024-z

INTRODUCTION

Previous studies have established that patients with chronic pain also have mental disorders, including anxiety [1–3]. Unlike common comorbidities, chronic pain and anxiety often contribute to each other's development [4–6]. Several studies have recently reported that ~40% of patients suffering from chronic pain still present anxiety after analgesic administration in the clinic [7, 8]. In other words, anxiety could be persistent even after chronic pain has been relieved by analgesics. However, the molecular mechanism of chronic pain-induced anxiety, especially after analgesic treatment, is less clear, making clinical therapeutic strategies difficult.

The ventromedial prefrontal cortex (vmPFC), which comprises the prelimbic cortex and infralimbic cortex, has been studied by many researchers in terms of anxiety, while it is also associated with pain [9–12]. Data from several studies suggest that anxiety induced by chronic pain enhances excitatory synaptic plasticity in the vmPFC [11–13], which involves *N*-methyl-*D*-aspartic acid receptors (NMDARs) and α-amino-3-hydroxy-5-methyl-4-isoxazolepropionic acid receptors (AMPARs), two ionotropic glutamate receptor subtypes. The pharmacological activation of the prelimbic cortex via NMDARs and activation of the infralimbic cortex via AMPAR-mediated glutamatergic neurotransmission in mice induce anxiety-like behaviours [12, 14, 15]. Synaptic plasticity in the brain is largely determined by changes in the surface expression of AMPARs, so-called AMPAR trafficking [16]. Four homologous major core subunits (GluA1-4) form heteromeric tetrameric complexes characterised as AMPARs [17]. Most AMPARs are GluA1/GluA2 or GluA2/GluA3 heteromeric complexes, but some are homomeric GluA1 complexes, and the augmentation of synaptic currents is associated with an increase in synaptic GluA1 and GluA2 levels [18, 19]. The findings in recent studies demonstrated that interfering with AMPAR surface diffusion markedly impaired stable excitatory postsynaptic potentials (EPSPs) and synaptic potentiation [20]; an activity-dependent decrease in mini-excitatory postsynaptic current (mEPSC) amplitude in spinal cord neurons was accompanied by a reduction in the accumulation of AMPARs at synapses [21]. All these results support the idea that AMPAR trafficking is vital to excitatory transmission.

[1]Department of Pharmacology, School of Pharmacy, Nanjing Medical University, Nanjing 211166, China; [2]The First Affiliated Hospital of Fujian Medical University, Longyan 364000, China; [3]Guangdong-Hong Kong-Macao Greater Bay Area Center for Brain Science and Brain-Inspired Intelligence, Guangzhou 510515, China and [4]Department of Medicinal Chemistry, School of Pharmacy, Nanjing Medical University, Nanjing 211166, China
Correspondence: Chun-xia Luo (chunxialuo@njmu.edu.cn)

Received: 1 August 2022 Accepted: 2 November 2022
Published online: 2 December 2022

SPRINGER NATURE © The Author(s), under exclusive licence to Shanghai Institute of Materia Medica, Chinese Academy of Sciences and Chinese Pharmacological Society 2022

S-nitrosylation of AMPAR-interacting proteins such as stargazin and N-ethylmaleimide sensitive factor (NeSF) contributes to AMPAR trafficking by augmenting the binding to AMPAR subunits [22, 23]. Stargazin can interact with all subtypes of AMPARs after S-nitrosylation and plays a vital role in regulating AMPAR trafficking and function [22]. NeSF mainly elicits enhanced surface expression of GluA2 [23].

Previously, we demonstrated that neuronal nitric oxide synthase (nNOS)-expressing neurons in the vmPFC of mice were the key to transforming chronic pain signals to anxiety behaviours [12], and the activation of nNOS depends on the interaction with postsynaptic density protein-95 (PSD-95) [24]. Additionally, we found that the downstream signalling pathway after nNOS-expressing neuronal activation was nitric oxide (NO) production and the enhancement of AMPAR-dependent excitatory synaptic transmission through AMPAR trafficking in the vmPFC [12]. However, the molecular mechanism of AMPAR trafficking, which mediates chronic pain-induced anxiety, remains unclear. Most importantly, the signal separation of anxiety from chronic pain following the activation of nNOS-expressing neurons in the vmPFC strongly suggests the possibility that the AMPAR-associated mechanism was implicated in persistent anxiety, which could not be relieved by analgesics. As a small molecular inhibitor we developed to disrupt the nNOS and PSD-95 interaction, ZL006 may be a potential drug for persistent anxiety. The verification of this possibility and the discovery of the critical molecule would promote the development of a specific strategy for this type of anxiety in the clinic.

In this study, we mimicked chronic pain-induced anxiety-like behaviours in mice using complete Freund's adjuvant (CFA) and established a protocol for screening mice with or without anxiety-like behaviours after analgesic administration. Moreover, we investigated the role of S-nitrosylation of the AMPAR binding protein stargazin in AMPAR trafficking and excitatory synaptic transmission in the vmPFC and determined whether this molecular mechanism is responsible for persistent anxiety. Finally, we determined the effect of ZL006 on anxiety-like behaviours in mice whose chronic pain was alleviated with analgesic treatment.

MATERIALS AND METHODS

Animals

Male young adult (6–7 weeks) C57BL/6 mice (Gempharmatech Co., Ltd, Nanjing, China) and nNOS-Cre mice (B6.129-Nos1$^{tm1(cre)Mgmj}$/J; The Jackson Laboratory; stock number: 017526) were used in experiments with virus microinjection, and male adult (8–9 weeks) mice were used in other experiments. All animals were maintained at a controlled humidity, room temperature (20 ± 2 °C), and 12 h (7:00 a.m. to 7:00 p.m.) light/dark cycle. Food and water were given ad libitum. The procedures of this study were approved by the Institutional Animal Care and Use Committee of Nanjing Medical University. All animal experiments were conducted according to the ARRIVE (Animal Research: Reporting of In Vivo Experiments) guidelines [25].

Chronic pain model

CFA (Sigma–Aldrich, catalogue #F5881) was used to induce chronic inflammatory pain in mice [11, 26]. Ten microlitres of CFA (1 mg/ml, dissolved in 85% paraffin oil and 15% mannide monooleate, heat-killed Mycobacterium tuberculosisin) was administered by subcutaneous injection into the planta of both hind paws after disinfection with 75% ethanol. Bilateral CFA injection instead of unilateral CFA injection was chosen to obtain more persistent anxiety in mice.

Anxiety-related behaviour tests

Anxiety-related behaviours of mice were assessed using the elevated plus maze (EPM) test and open field (OF) test or the novelty-suppressed feeding (NSF) test and light-dark box (LDB) test as described in our previous studies [12, 27]. Immediately after each test, the animal was transferred to its home cage. An interval of 30 min between two behavioural tests (OF and EPM or NSF and LDB) allowed the animals to rest. All these behavioural tests were carried out in a blinded manner.

The elevated plus maze (EPM) consists of two precarious arms (open without sidewalls, 30 × 5 cm^2) and two safe arms (closed by sidewalls, 30 × 5 cm^2, with end and sidewalls 15 cm high). These four arms are connected by a central platform (5 × 5 cm^2) 50 cm above the floor. Mice were released from the central platform, with their face pointing towards an open arm. Each mouse was allowed to explore the maze freely for 5 min. TopScan LITE software (Clever Sys Inc., Reston, VA, USA) was used to record and analyse animal behaviours. The locomotor activities of mice were assessed by their total number of entries into the four arms, and their anxiety levels were represented by the time spent in open arms.

An apparatus constructed of a plastic box (30 × 30 × 50 cm^3) was used to measure the activity of mice in the open field (OF) test. Each mouse was gently placed in a corner of the test arena and allowed to explore the open field freely for 5 min. The whole process of mouse exploration in the open field was recorded and analysed with TopScan LITE software (Clever Sys Inc.). The locomotor activities of mice were assessed by the total distance travelled in the open field, and their anxiety levels were represented by the time spent moving in the square region (15 × 15 cm^2) in the centre of the open field.

The novelty-suppressed feeding (NSF) testing apparatus consisted of a plastic box (50 × 50 × 20 cm^3) covered with ~2 cm wooden bedding, and a single pellet of food was placed on a white paper platform positioned in the brightly illuminated centre. All the food was removed from the home cage 24 h before behavioural testing. At the time of testing, each mouse was placed in a corner of the box, and the latency to eat (defined as the mouse sitting on its haunches and biting the pellet with the use of forepaws) was timed. The NSF test lasted 5 min, and the mice that timed out were assigned a latency of 300 s. The amount of food consumed by the mouse in 15 min was also measured, serving as a control for feeding behaviour.

The LDB test was performed by placing a mouse in a cage that had two chambers: one lit (20 × 30 × 40 cm^3) and one dark compartment (20 × 30 × 40 cm^3). Each mouse was initially placed on the lit side and allowed to move freely between sides for 4 min. The time spent in each compartment and the total distance between the two compartments were recorded.

Mechanical allodynia measurement

Von Frey monofilaments (Touch-Test TM Sensory Evaluator, North Coast Medical, Inc., Atlanta, GA, USA) were used to assess mechanical hypersensitivity [26]. The 50% paw withdrawal threshold in response to the mechanical stimulus was considered the criterion for the pain level. Before testing, mice were individually placed in a plastic cage (45 cm × 5 cm × 11 cm) with a wire mesh bottom and allowed to acclimate for 20 min. Von Frey filaments, ranging from 0.02 to 2 g, were applied perpendicular to the plantar surface with sufficient force in ascending order of strength to cause slight bending against the hind paw and held for 4 s. The 0.4 g stimulus was applied first. It was considered to have had a positive response if the rodent withdrew, licked, or shaked its paw. If a positive response was observed, the next smaller von Frey filament was used; otherwise, the next thicker filament was applied. The experimental procedures were performed in a blinded manner.

Recombinant AAVs and infection

The desired recombinant adeno-associated virus was infused bilaterally into the vmPFC of mice with a stereotaxic apparatus (Stoelting, Wood Dale, IL, USA) at a rate of 0.2 nl/s (1 × 10^{13} v.g./ml,

0.4 μl). AAV-CaMKIIα-stargazin(C302S)-3flag-T2A-mCherry and its control virus AAV-CaMKIIα-3flag-T2A-mCherry were both produced by GeneChem (Shanghai, China). The former expressed 3flag-tagged mouse stargazin with a point mutation of cysteine 302 serine. This mutant stargazin could not be activated by S-nitrosylation [22]. AAV-hSyn-DIO-hM3Dq-eGFP was a commercialised product from GeneChem (catalogue # AAV00071), which was used for chemogenetic stimulation of nNOS neurons in nNOS-Cre mice through Cre-dependent expression of the excitatory DREADD hM3Dq. AAV-hSyn-DIO-eGFP (OBiO, Shanghai, China, catalogue # HYMBH4883) was used for visualisation of nNOS neurons in nNOS-Cre mice. The desired AAVs were microinjected 3 weeks before behavioural tests. After the injection, the needle was maintained in place for an additional 10 min to facilitate the diffusion of the virus and then slowly withdrawn. The coordinates of the vmPFC were as follows: AP, +1.7 mm; ML, ±0.3 mm; DV,−2.3 mm.

Drugs and their administration

The anti-inflammatory analgesic ibuprofen (Smith Kline & French Laboratories Ltd, Tianjin, China) was dissolved in drinking water (1 mg/ml) [28] and administered from Day 3 after CFA injection [29]. Since the average daily drinking water intake of each mouse we measured was 4 ml, the daily dose of ibuprofen for each mouse was ~4 mg (equivalent to the clinical dose). A small molecular inhibitor of nNOS-PSD-95, ZL006, was designed and synthesised in our laboratory [24]. ZL006 was dissolved in 0.9% saline containing 0.8% $NaHCO_3$ as we described previously [24, 30]. In vivo, mice with persistent anxiety that were screened out were injected intraperitoneally with ZL006 (20 mg/kg, once a day) or its vehicle over 5 consecutive days. In vitro, ZL006 (10 μM) or its vehicle was added simultaneously with clozapine-N-oxide (CNO, Tocris Bioscience, catalogue #4936, 10 μM). For NO donor DETA/NONOate delivery, a stainless-steel guide cannula (26 gauge, 1.5 mm, RWD Life Science) was implanted into the vmPFC (AP, +1.7 mm; ML, ±0.3 mm) just after AAV microinjection. The cannula was fixed to the skull with adhesive luting cement and acrylic dental cement. Following surgery, a stainless-steel obturator was inserted into the guide cannula to avoid obstruction until microinjection was made. Mice were briefly head restrained while the stainless-steel obturator was removed, and an injection tube (30 gauge, 2.3 mm, RWD Life Science) was inserted into the guide cannula. A dose of DETA/NONOate (Sigma–Aldrich, catalogue #A5581) was slowly infused at a flow rate of 0.2 μl/min to a total volume of 1 μl. The concentration of DETA/NONOate (100 μM) was the same as that administered in our previous work [12, 31]. Following injection, the injection cannula was left in place for 5 min to reduce backflow. The stainless-steel obturator was subsequently reinserted into the guide cannula.

Immunofluorescence and cell counting

The samples used for immunofluorescence were randomly selected from each group after the behavioural tests. The details of immunofluorescence for brain sections were the same as in previous studies [12, 32]. The primary antibodies used in this study were mouse anti-flag (1:400; Sigma–Aldrich, catalogue #F1804, RRID: AB_262044), rabbit anti-CaMKII alpha (1:50; Abcam, catalogue #ab103840, RRID: AB_10900968), guinea pig anti-c-Fos (1:200; Synaptic System, catalogue #226-004, RRID: AB_2619946) and rabbit anti-nNOS (1:400; Thermo Scientific, catalogue #61-7000, RRID: AB_2313734). The secondary antibodies used were goat anti-mouse Alexa Fluor® 488 (1:400; Jackson ImmunoResearch Laboratories, catalogue #115-545-003, RRID: AB_2338840), goat anti-rabbit Alexa Fluor® 647 (1:200; Jackson ImmunoResearch Laboratories, catalogue #111-605-003, RRID: AB_2338072), goat anti-guinea pig Alexa 488 (1:200; Abcam, catalogue #ab150185, RRID: AB_2736871) and goat anti-rabbit Cy3 (Jackson ImmunoResearch Laboratories, catalogue #111-165-003; RRID: AB_2338000). Finally, brain slices were counterstained with Hoechst 33258 (1:200; Sigma–Aldrich, catalogue #B1155, CAS number: 23491-45-4) to label the nuclei.

Cell counting was conducted on every fourth section in a series of 40-μm coronal sections throughout the vmPFC. The fluorescent images were acquired at 40×. To obtain the ratio of c-Fos^+&$nNOS^+$ cells to $nNOS^+$ cells, the counts of c-Fos^+&$nNOS^+$ cells or $nNOS^+$ cells from all sampled sections of one animal were summed, and the ratio was calculated.

Fluorescent in situ hybridisation (FISH)

We performed FISH using an RNAscope assay kit (Advanced Cell Diagnostics, Newark, CA, USA), and the details were the same as before [12]. Probes used: RNAscope® Probe-Mm-Nos1, RNAscope® Probe-EGFP-C2. These two probes were visualised by Cy3 and Cy5, respectively. An RNAscope® 3-plex negative control probe was used to confirm the specificity of the labelling.

Western blot analysis

The samples used for Western blotting were randomly selected from each group after the behavioural tests. Western blot analysis was performed as previously described [12, 32]. The primary antibodies we used were as follows: rabbit anti-GluA1 (1:4000; Abcam, catalogue #ab109450, RRID: AB_10860361), rabbit anti-GluA2 (1:4000; Abcam, catalogue #ab133477, RRID: AB_2620181), mouse anti-GAPDH (1:4000; KangChen Biotech, catalogue #KC-5G4, RRID: AB_2493106), rabbit anti-β-tubulin (1:4000; Bioworld Technology, catalogue #BS1482 M), rabbit anti-PSD-95 (1:1000; Cell Signaling Technology, catalogue #2507, RRID: AB_561221), rabbit anti-nNOS (1:1000; Thermo Scientific, catalogue #61-7000, RRID: AB_2313734), rabbit anti-NeSF (1:4000; Abcam, catalogue #ab87155, RRID: AB_10674097) and rabbit anti-stargazin (1:1000; Millipore, catalogue #07-577, RRID: AB_310726). The membranes were processed with enhanced chemiluminescence Western blotting detection reagents (Bio-Rad, Hercules, CA, USA) after incubation with appropriate horseradish peroxidase-linked secondary antibodies.

Extraction of membrane protein fractions

A kit (catalogue #71772-3) purchased from Merck (Germany) was used to extract membrane protein fractions according to the manufacturer's protocol as we previously described [33]. The membrane proteins were quantitatively analysed by normal Western blot analysis. The tissues collected for measuring membrane proteins were chosen randomly from each group after behavioural tests.

Biotin-switch assay

For the biotin-switch assay, the vmPFC tissues of mice were collected randomly from each group after behavioural tests. This assay was performed in the dark as previously reported [12, 34]. Briefly, tissues were lysed in HEN buffer (250 mM HEPES, 1 mM EDTA, and 100 mM neocuproine) and adjusted to contain 0.4% CHAPS. Samples were homogenised, and free cysteines were blocked for 1 h at 50 °C in three volumes of blocking buffer [HEN buffer plus 2.5% SDS (HENS)] containing methyl methanethiosulfonate (200 mM). Proteins were precipitated with acetone at −20 °C and resuspended in 300 μl HENS buffer. Proteins were incubated at 30 °C for 1 h after adding fresh ascorbic acid (20 mM) and biotin-HPDP (1 mM; Thermo Scientific, catalogue #21341). Biotinylated proteins were precipitated with acetone at −20 °C and resuspended in 250 μl HENS buffer plus 500 μl neutralisation buffer (20 mM HEPES, 100 mM NaCl, 1 mM EDTA, 0.5% Triton X-100) and precipitated with 30 μl prewashed avidin-affinity resin beads (Sigma–Aldrich, catalogue #85881) at 4 °C overnight. The beads were washed five times at 4 °C using neutralisation buffer containing 600 nM NaCl. Biotinylated proteins were eluted using 35 μl of elution buffer (20 mM HEPES, 100 mM NaCl, 1 mM EDTA,

100 mM β-mercaptoethanol) and heated at 100 °C for 8 min in reducing SDS–PAGE loading buffer.

Coimmunoprecipitation
As we previously described [27, 35], the vmPFC tissues were lysed in buffer containing 50 mM Tris-HCl (pH 7.4), 150 mM NaCl, 1 mM EDTA-Na, 1% NP-40, 0.02% sodium azide, 0.1% SDS, 0.5% sodium deoxycholate, 1% PMSF, 1‰ aprotinin, 1‰ leupeptin, and 0.5‰ pepstatin A. The lysates were centrifuged at 12,000 × *g* for 15 min at 4 °C. The supernatant (200 μl) was incubated for 8 h at 4 °C with mouse anti-nNOS (1:100; BD Biosciences, catalogue #610309, RRID: AB_397700), and then the protein G-Sepharose beads (Sigma–Aldrich) were added to the target antibody-conjugated supernatant for incubation overnight at 4 °C. Immune complexes were isolated by centrifugation and washed seven times with 1×PBS, and bound proteins were eluted by heating at 100 °C in 1× loading buffer for 10 min.

Electrophysiology
Mice randomly chosen from each group were anaesthetised with ethyl ether at days 1–3 after behavioural tests and then perfused with 10 ml ice-cold oxygenated (95% O_2 and 5% CO_2) dissection buffer that contained (in mM): 2.5 KCl, 0.5 $CaCl_2$, 7 $MgCl_2$, 7.3 NaH_2PO_4, 25 $NaHCO_3$, 1.3 Na-ascorbate, 0.6 Na-pyruvate, 110 choline chloride, 20 glucose. Brains were quickly removed into the same solution. Coronal brain slices (350 μm) containing the vmPFC were prepared using a vibratome, and the slices were incubated in an interface-style chamber containing normal artificial cerebrospinal fluid (ACSF) composed of 10 mM glucose, 125 mM NaCl, 2.5 mM KCl, 2 mM $CaCl_2$, 1.3 mM $MgCl_2$, 1.3 mM NaH_2PO_4, 25 mM $NaHCO_3$, 1.3 mM Na-ascorbate, and 0.6 mM Na-pyruvate (gassed with 95% O_2/5% CO_2) at 25 °C for at least 1 h. All the following electrophysiological recordings were performed on pyramidal neurons in layer 2/3, the activity of which is highly related to anxiety behaviours [11, 36, 37].

Miniature EPSC recording. Mini EPSCs were recorded by whole-cell patch clamp. Infrared oblique illumination (Olympus X51W; Hamamatsu CCD camera C11440) was used to visualise pyramidal neurons in the vmPFC. Patch electrodes (6–8 MΩ) were filled with pipette solution containing (in mM) 132.5 Cs-gluconate, 17.5 CsCl, 2 $MgCl_2$, 0.5 ethylene glycol bis(2-aminoethyl)tetraacetic acid (EGTA), 10 HEPES, 4 ATP, and 5 QX-314 (pH 7.3). For voltage-clamp recordings, mEPSCs were recorded at −60 mV. To study mEPSC activity in isolation, all recordings were performed in the presence of 0.5 μM TTX, 20 μM BMI, and 50 μM AP-5 to block action potentials and isolate AMPAR-mediated currents. The amplitude and frequency of mEPSCs were analysed with Mini software (Synaptosoft Inc., Fort Lee, NJ, USA).

AMPA/NMDA ratio recording. Pyramidal neurons in the vmPFC were visualised using a fluorescent and an infrared-DIC optical system combined with a CCD camera and monitor. Microelectrodes (6–8 MΩ) were filled with internal pipette solution containing 132.5 mM Cs-gluconate, 17.5 mM CsCl, 2 mM $MgCl_2$, 0.5 mM EGTA, 10 mM HEPES, 4 mM ATP, and 5 mM QX-314. In this experiment, 20 μM BMI was added to the ACSF to block inhibition. AMPA receptor-mediated EPSCs were calculated by averaging 15 EPSCs at −70 mV and measuring the peak compared with the baseline. NMDA receptor-mediated EPSCs were calculated by averaging 15 EPSCs at +40 mV and measuring the amplitude 50 ms after the stimulation compared with the baseline.

Action potential recording. For action potential recording, pipettes (4–6 MΩ) were filled with electrode internal solution containing (in mM) 70 K-gluconate, 70 KCl, 2 NaCl, 2 $MgCl_2$, 10 HEPES, 1 EGTA, 2 MgATP and 0.3 Na_2GTP (pH 7.3). To confirm the functionality of expressed hM3Dq, APs of hM3Dq-expressing neurons in the vmPFC of nNOS-Cre mice were recorded by whole-cell current clamp. An appropriate current was injected into the patched neurons to induce spiking. After 3 min of continuous recording, CNO (5 μM) was added to aCSF for the following recording. Neuronal excitability of nNOS-expressing neurons in the vmPFC from the anxious and non-anxious mice was assessed using the input–output curve measured from the changes in membrane potential (presence of action potentials) evoked by current steps (0–140 pA, increasing in increments of 10 pA) in current-clamp mode.

Cell culture and NO level detection
NO levels were measured in living neurons cocultured with glia using DAF-FM DA as we described previously [35]. Cocultures were prepared from the cortex of neonatal nNOS-Cre mice (1-day-old) and seeded at 5×10^4 cells/cm^2 on dishes coated with 10 μg/ml polyornithine (Sigma–Aldrich) in a mixed medium with 50% Neurobasal medium (Invitrogen) containing 2% B27 supplement (Invitrogen) and 50% DMEM/F12 (Invitrogen) containing 10% FBS. Cocultures were infected with LV-hSyn-DIO-hM3Dq-mCherry (5×10^8 TU/ml, BrainVTA, Wuhan, China) at day 4 in vitro. CNO (10 μM) was applied at day 10 to specifically activate nNOS neurons in cocultures through Cre-dependent hM3Dq expression in nNOS neurons in the presence or absence of ZL006 (10 μM). Thirty minutes after CNO incubation, 10 μM DAF-FM DA (Calbiochem, catalogue #251520-M) and 0.5 μg/ml Hoechst 33258 (Sigma–Aldrich, catalogue #B1155) were applied in the dark incubator. Sixty minutes after incubation, the production of NO in living cells was examined, and fluorescent signals of NO produced by cells were captured with a living cell imager (Zeiss, Oberkochen, Germany).

Data and statistical analysis
No sample-size calculation was performed in this study. The sample size was 12–16 mice for animal behavioural tests (except screening experiments), 5 mice for biochemical measurements and 8–15 neurons (from 4 mice) for electrophysiology, according to our prior experience [12, 27, 30, 31]. To obtain sufficient anxious and non-anxious mice after ibuprofen treatment in the screening experiment, 70–80 mice were included in the CFA + IBU group. The accurate sample size is given in each figure legend. No data were excluded from the analysis unless accidental events occurred. The details of excluded animals, if any, are provided in the figure legend.

All data included in the statistics were imported into Prism 8.0.2 (GraphPad Software, La Jolla, CA, USA). Data were tested for normality using the D'Agostino-Pearson test and Kolmogorov–Simimov test and for variance using the *F* test. When the data followed a normal distribution and passed the *F* test, the results were analysed by unpaired two-tailed Student's *t* tests for comparison between two groups and Tukey's test following ordinary one-way ANOVA for comparison among multiple groups. When the data did not follow a normal distribution, a two-tailed Mann–Whitney *U* test was used to compare two groups, and Dunn's test following Kruskal–Wallis ANOVA was used to compare multiple groups. When the data followed a normal distribution but did not pass the *F* test, two-tailed Welch's *t* test was used to compare two groups, and Games-Howell's test ($n > 50$) or Tamhane's T2 ($n < 50$) test following Brown-Forsythe and Welch ANOVA was used to compare multiple groups. Cumulative probability plots were produced for the analysis of mEPSCs (Mini Analysis software 6.0), and statistical analysis was performed on mean values. Data are presented as the mean ± SEM, and $P < 0.05$ was considered statistically significant.

RESULTS

Chronic pain-induced anxiety is persistent after analgesic administration
A large number of chronic pain patients still suffer from anxiety, although they have received analgesic treatment [7, 8]. We observed a similar phenomenon in mice as well. CFA was used to

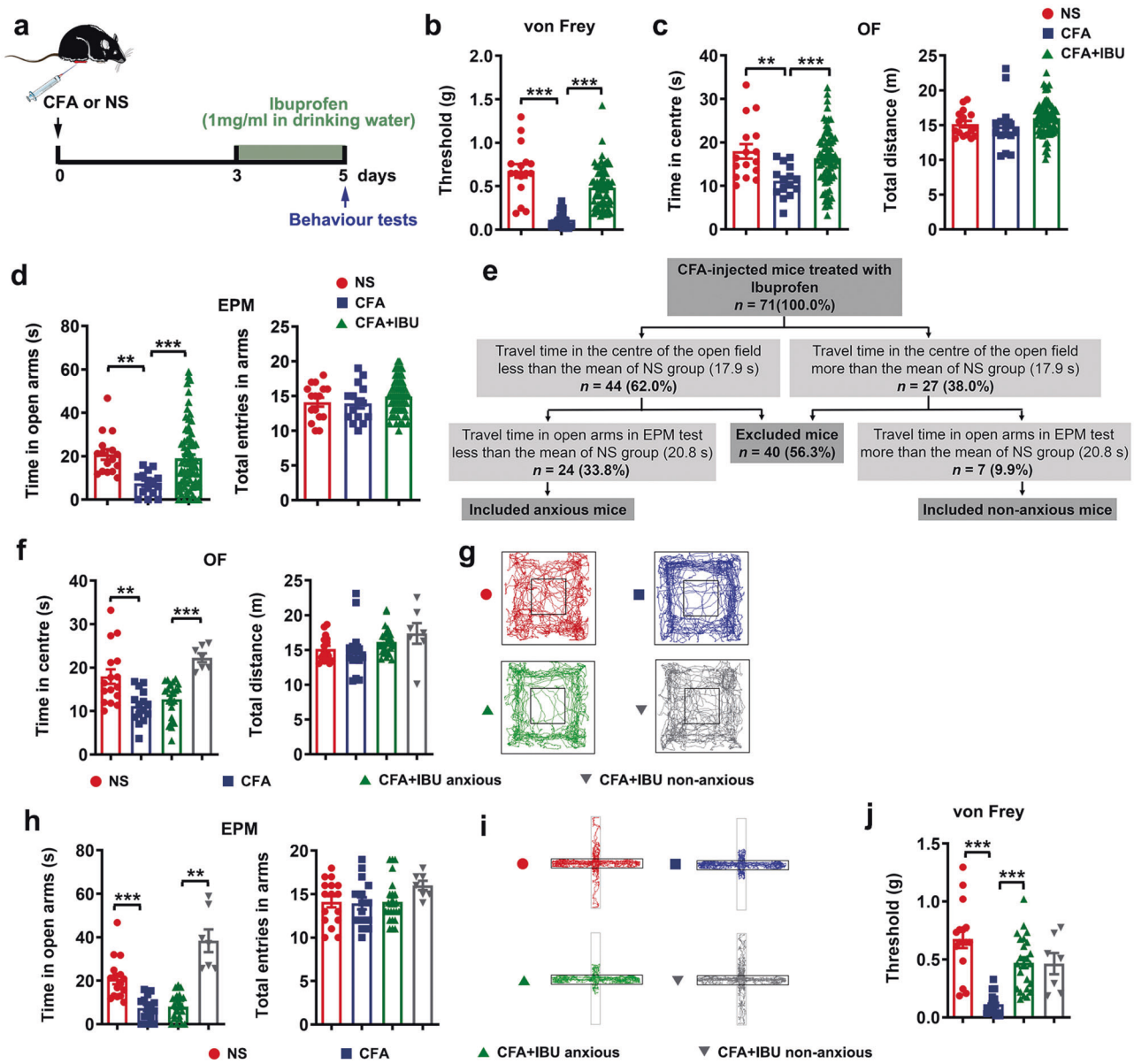

Fig. 1 Chronic pain-induced anxiety-like behaviours in mice treated with ibuprofen. a Scheme of the experimental design. Withdrawal threshold of the hind paw in von Frey tests (**b**), time in centre (**c**, left) and total distance (**c**, right) in the OF test, and time in open arms (**d**, left) and total entries in arms (**d**, right) in EPM tests at Day 5 after CFA injection (with 2-day ibuprofen administration). $n = 16$, 15 and 71, respectively. **e** Protocol for selecting the persistent anxiety mice and the non-anxious mice after 2 days of ibuprofen administration based on their behaviours in the OF test and EPM test at Day 5 after CFA injection. Time in centre (**f**, left), total distance (**f**, right) and representative traces of mice location (**g**) in OF tests, time in open arms (**h**, left), total entries in arms (**h**, right) and representative traces of mouse location (**i**) in EPM tests, and withdrawal threshold of the hind paw in von Frey tests (**j**) after 2-day ibuprofen administration for the new groups after filter. $n = 16$, 15, 24 and 7, respectively. Data are the mean ± SEM; $^{**}P < 0.01$, and $^{***}P < 0.001$ (Tukey's test following ordinary one-way ANOVA for **d** (right), Games-Howell's test following Brown–Forsythe and Welch ANOVA for **c** (left), **f** (left), **h** (left) and **j**, and Dunn's test following Kruskal–Wallis ANOVA for **b**, **c** (right), **d** (left), **f** (right) and **h** (right)).

induce chronic inflammatory pain [11, 12, 38]. In our previous study, we established that mice exhibited significant anxiety-like behaviours 3 days after CFA injection into the plantar surface of the hind paws [12]. Therefore, we treated mice with ibuprofen (1 mg/ml) in their drinking water from Day 3 after CFA injection [28, 29] and tested mechanical allodynia and anxiety-like behaviours at Day 5 (Fig. 1a). The results showed that ibuprofen treatment completely rescued the CFA-induced reduction of paw withdrawal threshold to mechanical stimuli, suggesting obvious analgesia (Fig. 1b). However, time in the centre in the open field (OF) test (Fig. 1c) and time in the open arms in the elevated plus maze (EPM) test (Fig. 1d) observed in ibuprofen-treated mice displayed a high variation across the levels of the NS group and CFA group. These discrete data implied that chronic pain-induced anxiety was alleviated by ibuprofen treatment only in some mice. Additionally, total distance in the OF (Fig. 1c) and total arm entries in the EPM (Fig. 1d) among groups were similar, indicating the locomotor activities were not significantly changed.

To screen out mice with persistent anxiety-like behaviours after analgesic administration, we designed a protocol. As shown in Fig. 1e, a total of 71 CFA-injected mice were treated with ibuprofen. First, based on the average travel time (17.9 s) in the centre of the OF test of NS-injected mice, 44 (62.0%) mice that travelled less than the mean distance of the NS group were initially

classified as anxious, and the other 27 (38.0%) mice were classified as non-anxious. Then, we used the average travel time (20.8 s) in the open arms in the EPM test of NS-injected mice as another standard for screening anxious mice. Among 44 initial anxious mice, 24 (33.8%) mice that travelled less than the mean time of the NS group were finally included in the anxious group, and 7 (9.9%) out of 27 initial non-anxious mice that travelled more than the mean time of the NS group were finally included in the non-anxious group. Additionally, 40 (56.3%) mice were excluded from either group, although some of them also exhibited anxiety-like or anxiolytic-like behaviours. We reanalysed the behavioural results according to the new four groups. Ibuprofen-treated mice included in the anxious group showed similar anxiety levels as CFA-injected mice without ibuprofen treatment in the OF (Fig. 1f, g) and EPM (Fig. 1h, i) tests, although ibuprofen significantly increased the pain threshold (Fig. 1j). In contrast, the time spent in the centre of the OF (Fig. 1f, g) and the time spent in the open arms of the EPM (Fig. 1h, i) by anxious mice were completely separate from the non-anxious mice, although equal analgesic effects of ibuprofen occurred in both groups (Fig. 1j). Similar locomotor activities were observed in each group (Fig. 1f–i).

Enhanced AMPAR trafficking and function in the vmPFC are associated with persistent anxiety

What determined the difference between anxious mice and non-anxious mice after analgesic administration? We have reported the crucial role of AMPARs in the vmPFC for chronic pain-induced anxiety-like behaviours [12]. In this study, we measured the expression levels of GluA1 and GluA2, the dominant subunits of AMPARs, on the plasma membrane surface in the vmPFC of ibuprofen-treated mice and found a difference between the anxious group and the non-anxious group. As shown in Fig. 2a–c, CFA injection significantly upregulated GluA1 membrane expression. This upregulation was not substantially changed in the CFA + IBU anxious group but was dramatically reversed in the CFA + IBU non-anxious group. A similar difference was observed when the membrane expression of GluA2 subunits was examined (Fig. 2d–f). Moreover, AMPAR-dependent mini-excitatory postsynaptic currents (mEPSCs) and the AMPA/NMDA ratio were recorded on pyramidal neurons in the vmPFC of mice to assess AMPAR function. In agreement with the finding from AMPAR trafficking, the mEPSC amplitude augmentation induced by CFA did not obviously change in the CFA + IBU anxious group but markedly decreased in the CFA + IBU non-anxious group (Fig. 2g, h). The frequency of mEPSCs in all groups was not obviously different (Fig. 2g, i). The data from the AMPA/NMDA ratio further confirmed the difference in AMPAR function between ibuprofen-treated anxious mice and non-anxious mice (Fig. 2j, k). Together, these results suggested that persistent enhancement of AMPAR trafficking to the plasma membrane and AMPAR-dependent excitatory synaptic transmission in the vmPFC contributed to persistent anxiety-like behaviours that could not be relieved by analgesics after chronic pain.

S-nitrosylated stargazin mediates AMPAR trafficking and function in the vmPFC

NO regulates AMPAR trafficking by targeting the AMPAR-interacting proteins stargazin and NeSF. S-nitrosylation of these two proteins mainly enhanced the surface expression of GluA1 and GluA2 [12, 22, 23]. Therefore, we examined the S-nitrosylation levels of stargazin and NeSF in the vmPFC of anxious mice and non-anxious mice after ibuprofen treatment. Consistent with the results from the AMPAR membrane expression, the increased S-nitrosylation level of stargazin in the vmPFC by CFA injection was not altered in CFA + IBU anxious mice but was significantly decreased in CFA + IBU non-anxious mice (Fig. 3a–c). Similarly, there was a difference in S-nitrosylated NeSF between anxious mice and non-anxious mice, although the difference was not significant (Fig. 3a–c).

We hypothesised that S-nitrosylation of stargazin plays a critical role in chronic pain-induced anxiety by enhancing AMPAR-dependent excitatory synaptic transmission in pyramidal neurons of the vmPFC. To test this hypothesis, we generated a recombinant AAV-CaMKIIα-stargazin(C302S)-3flag-T2A-mCherry to express mutant stargazin(C302S), which could not be activated by S-nitrosylation [22]. The virus was microinjected into the vmPFC of mice to express exogenous stargazin (C302S) in pyramidal neurons through the CaMKIIα promoter (Fig. 4a). Three weeks later, accurate and effective expression of stargazin (C302S) was confirmed (Fig. 4b–d; Supplementary Fig. S1). A biotin-switch assay further verified that the exogenous expression of stargazin (C302S) significantly suppressed the S-nitrosylation of endogenous stargazin induced by CFA (Fig. 4e, g, h). Increased stargazin levels resulted from the expression of stargazin (C302S) (Fig. 4e, f). To determine whether the role of S-nitrosylated stargazin in regulating chronic pain-induced anxiety is associated with enhanced AMPAR trafficking in the vmPFC, we measured the surface expression of the AMPAR subunit GluA1 in stargazin (C302S)-overexpressing vmPFC 3 days after CFA injection when chronic pain-induced anxiety-like behaviours were obvious. As expected, stargazin (C302S) significantly inhibited membrane GluA1 in CFA-injected mice, with no influence on the total GluA1 level (Fig. 4i–k). Furthermore, we recorded AMPAR-dependent mEPSCs and the AMPAR/NMDAR ratio on pyramidal neurons in the vmPFC. For the AAV-infected groups, recordings were performed on mCherry$^+$ pyramidal neurons (Fig. 4l). Compared to the AAV-CaMKIIα-3flag-T2A-mCherry-infected group, the amplitude of mEPSCs in the AAV-CaMKIIα-stargazin(C302S)-3flag-T2A-mCherry-infected group was markedly reduced, and no significant change in the frequency of mEPSCs was observed among the groups (Fig. 4m–o). Exogenous stargazin (C302S) also reversed the AMPAR/NMDAR ratio in CFA-injected mice (Fig. 4p, q). Together, these results suggested that S-nitrosylated stargazin mediated AMPAR trafficking and synaptic transmission in the vmPFC, which might contribute greatly to chronic pain-induced anxiety, including persistent anxiety, after analgesic administration.

S-nitrosylation of stargazin is necessary for chronic pain-induced persistent anxiety

Next, we investigated whether S-nitrosylated stargazin mediated chronic pain-induced anxiety-like behaviours. AAV-CaMKIIα-stargazin(C302S)-3flag-T2A-mCherry was microinjected into the vmPFC 18 days before CFA injection to suppress the S-nitrosylation of stargazin in pyramid neurons (Fig. 5a). The behavioural tests showed that the expression of stargazin (C302S) in the vmPFC markedly reversed the anxiety-like behaviours induced by CFA (OF: Fig. 5b; EPM: Fig. 5c). Mice in each group showed similar locomotor activities (Fig. 5b, c). Therefore, S-nitrosylation of stargazin is critical to regulating the anxiety-like behaviours induced by chronic pain. No analgesic effect was observed when stargazin (C302S) was expressed in the vmPFC (Fig. 5d), which was consistent with our previous finding that NO in the vmPFC regulated anxiety without being implicated in hyperalgesia.

Then, we explored the role of S-nitrosylated stargazin in chronic pain-induced persistent anxiety after analgesic treatment. After 2 days of ibuprofen treatment, anxious mice were screened using the protocol described in Fig. 1e. AAV-CaMKIIα-stargazin(C302S)-3flag-T2A-mCherry was microinjected into the vmPFC, and mechanical allodynia and anxiety-like behaviours were tested 14 days after AAV microinjection (Fig. 5e). Fourteen days after AAV microinjection was chosen as the duration to balance the effective expression of AAV-mediated exogenous proteins and the spontaneous attenuation of CFA-induced pain (20 days after CFA injection). Ibuprofen was administered consecutively after screening to maintain effective analgesia in mice with persistent anxiety (Fig. 5f; Supplementary Fig. S2a). As expected, CFA-induced

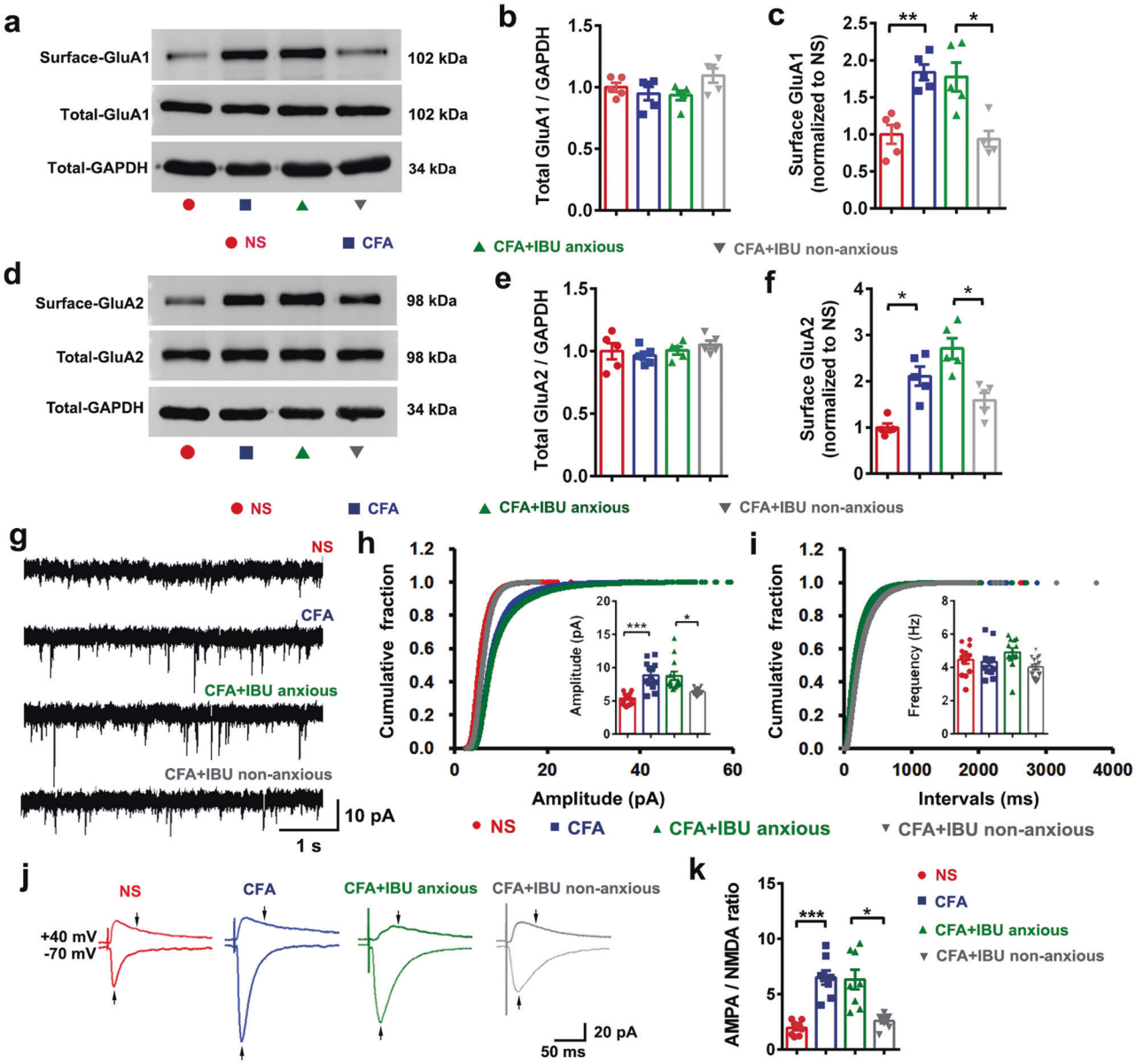

Fig. 2 Enhanced AMPAR trafficking and synaptic transmission in the vmPFC of mice with chronic pain-induced persistent anxiety. Representative Western blots (**a**) and dot plots showing total (**b**) and surface (**c**) protein levels of GluA1 after 2 days of ibuprofen administration. $n = 5$ for each group. Representative Western blots (**d**) and dot plots showing total (**e**) and surface (**f**) protein levels of GluA2 after 2 days of ibuprofen administration. $n = 5$ for each group. **g** Representative traces of mEPSCs recorded with the whole-cell patch clamp on layer 2/3 pyramidal neurons in the vmPFC of mice after 2 days of ibuprofen administration. Cumulative fraction plots of mEPSC amplitude (**h**, mean amplitude in inset) and interevent intervals (**i**, mean frequency in inset). $n = 13$ neurons (from 4 mice) for each group. **j** Representative traces of eEPSCs in the presence of BMI (20 μM) recorded with the whole-cell patch-clamp on layer 2/3 pyramidal neurons in the vmPFC of mice after 2 days of ibuprofen administration. Arrows indicate that AMPAR-EPSCs were measured at their peak at a holding potential of −70 mV, and NMDAR-EPSCs were measured 50 ms after stimulation at a holding potential of +40 mV. **k** Dot plot showing the AMPA/NMDA ratio. $n = 8$ neurons (from 4 mice) for each group. Data are expressed as the mean ± SEM; $^{*}P < 0.05$, $^{**}P < 0.01$, and $^{***}P < 0.001$ (Tukey's test following ordinary one-way ANOVA for **b** and **e**, Tamhane's T2 test following Brown-Forsythe and Welch ANOVA for **c**, **f**, **k** and Dunn's test following Kruskal–Wallis ANOVA for **h** (inset) and **i** (inset)).

anxiety-like behaviours that were persistent in AAV-CaMKIIα-3flag-T2A-mCherry-infected mice with regular analgesic administration were dramatically attenuated in AAV-CaMKIIα-stargazin(C302S)-3flag-T2A-mCherry-infected mice (OF: Fig. 5g; EPM: Fig. 5h). This effect was not due to spontaneous recovery because CFA-induced mechanical allodynia and anxiety-like behaviours were persistent without treatment (Supplementary Fig. S2a-c). Taken together, our results demonstrated that S-nitrosylation of stargazin was necessary for chronic pain-induced anxiety, especially persistent anxiety, after analgesic treatment.

NO derived from activated nNOS-expressing neurons is increased in mice with persistent anxiety

Although S-nitrosylated stargazin is critical, it is not an ideal therapeutic target. Thus, we turned to NO, which caused S-nitrosylation. As shown in Fig. 6, persistent anxiety mice showed more nNOS-expressing neurons colabelled with c-Fos (a widely used indicator of cell activation) in the vmPFC 1 h after behaviour tests (Fig. 6a, b) than non-anxious mice, and the vmPFC nNOS-expressing neurons in persistent anxiety mice had greater action potential (AP) firing and higher sensitivity in

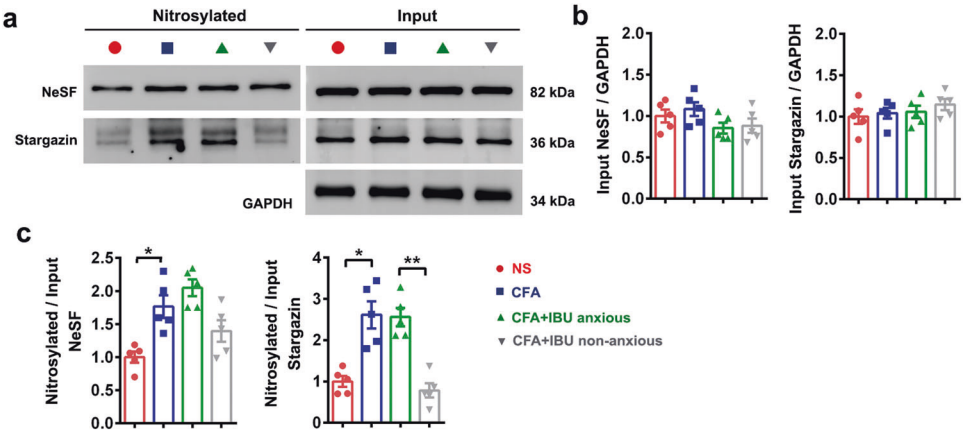

Fig. 3 Enhanced S-nitrosylation levels of AMPAR-interacting proteins in the vmPFC of mice with chronic pain-induced anxiety. **a** Representative blots of the biotin-switch assay. **b** Input levels of NeSF and stargazin. $n = 5$ for each group. **c** S-nitrosylated levels of NeSF and stargazin. $n = 5$ for each group. Data are the mean ± SEM; $^{*}P < 0.05$, and $^{**}P < 0.01$ (Tukey's test following ordinary one-way ANOVA for **b** and Tamhane's T2 test following Brown-Forsythe and Welch ANOVA for **c**).

response to depolarising step currents (Fig. 6c-f) than those in non-anxious mice. This implied activation of nNOS-expressing neurons and possible NO production in mice with persistent anxiety. Additionally, we confirmed that the NO donor DETA/NONOate microinjected into the vmPFC induced anxiety-like behaviours and that stargazin (C302S)-expressing AAV completely reversed the effect of DETA/NONOate (Supplementary Fig. S3a–c).

To further confirm increased NO production in activated nNOS-expressing neurons and explore the contribution to persistent anxiety, we infused an adeno-associated virus expressing hM3Dq (AAV-hSyn-DIO-hM3Dq-eGFP) into the vmPFC of nNOS-Cre mice to stimulate nNOS-expressing neurons through chemogenetics (Fig. 7a). hM3Dq is a clozapine N-oxide (CNO)-based excitatory designer receptor exclusively activated by designer drugs (DREADD). Three weeks after microinjection of the virus, hM3Dq-eGFP, identified as green fluorescence, was abundantly expressed in the vmPFC (Fig. 7b) and was colocalized with nNOS-expressing neurons (Fig. 7c). We also verified that Cre-dependent mRNA expression was specific to nNOS neurons using fluorescence in situ hybridisation (FISH) (Supplementary Fig. S4). Moreover, efficient stimulation of hM3Dq-expressing neurons was confirmed by increased AP firing after applying a CNO bath to brain slices (Fig. 7d). Then, we tested animal behaviours. Thirty minutes after CNO or NS administration, chemogenetic activation of vmPFC nNOS-expressing neurons resulted in significant anxiety-like behaviours in the OF test (Fig. 7e) and EPM test (Fig. 7f) with no influence on locomotor activities (Fig. 7e, f) or nociception (Fig. 7g). More importantly, coimmunoprecipitation experiments revealed that the interaction of nNOS with PSD-95 was obviously increased in the vmPFC when nNOS-expressing neurons were activated and anxiety-like behaviours were induced by CNO (Fig. 7h, i). Since the catalytic activity of nNOS depends on its association with PSD-95 [24], we wondered whether this enhanced interaction of nNOS with PSD-95 contributes to NO production. For an intuitive observation of NO released by the activated nNOS-expressing neurons, we then used DAF-FM DA to label NO in living neuronal and glial cocultures derived from nNOS-Cre mice and infected with LV-hSyn-DIO-hM3Dq-mCherry (Fig. 7j). As shown in Fig. 7k, obviously elevated NO levels were observed in chemogenetically activated nNOS-expressing neurons (mCherry^{+}). Together, these results suggested that the nNOS-PSD-95 interaction and NO production in the activated vmPFC nNOS-expressing neurons of anxious mice might be promising targets other than stargazin.

ZL006 alleviates chronic pain-induced persistent anxiety

To examine whether disrupting the nNOS-PSD-95 interaction prevents chronic pain-induced persistent anxiety, we used ZL006 (5-(3,5-dichloro-2-hydroxybenzylamino)-2-hydroxybenzoic acid), a specific nNOS-PSD-95 interaction inhibitor designed and synthesised in our previous study [24, 30]. First, we verified its inhibitory effect on NO production in nNOS-expressing neurons in vitro (Fig. 8a). Then, we treated CFA-induced persistent anxiety mice with ZL006 (20 mg/kg, ip., once a day) for 5 consecutive days (Fig. 8b) after screening with the protocol described in Fig. 1e. The biotin-switch assay demonstrated reduced S-nitrosylation levels of stargazin (Fig. 8c, d) and NeSF (Fig. 8c, e) in the vmPFC of ZL006-treated mice compared to vehicle-treated mice. Moreover, the novelty-suppressed feeding (NSF) test and light-dark box (LDB) test were performed to evaluate the anxiolytic effects of ZL006. These two new tests in addition to the OF test and EPM test in screening were chosen to avoid the possible influence of repeating the same behavioural tests in the short term (5 days). The results indicated that ZL006 substantially reduced the anxiety-like behaviours that were persistent after ibuprofen administration, as shown by the increased time spent in the light side in the LDB test (Fig. 8f) and the decreased latency to feed in the NSF test (Fig. 8g), with no influence on locomotor activities (Fig. 8f) or feeding behaviours (Fig. 8g). Additionally, ibuprofen-induced analgesia could not be further augmented by ZL006 because the pain threshold had been increased to normal levels (Fig. 8h; Supplementary Fig. S5a), and the ZL006-induced anxiolytic effect was not due to spontaneous recovery because CFA-induced anxiety was persistent without treatment (Supplementary Fig. S5b, c). Thus, the nNOS-PSD-95 interaction in nNOS-expressing neurons promoted the activation of the nNOS-NO pathway, resulting in persistent S-nitrosylation in the vmPFC of mice with persistent anxiety. This suggested that nNOS-PSD-95 inhibitors could serve as potential medicines for persistent anxiety caused by chronic pain.

Finally, we examined whether ZL006 would relieve both chronic pain and its comorbidity anxiety in mice without ibuprofen treatment regarding the analgesic effect of ZL006 [30]. ZL006 (20 mg/kg, ip., once a day) was administered for 5 consecutive days from Day 3 after CFA injection (Supplementary Fig. S6a). The results showed that either mechanical allodynia (Supplementary Fig. S6b) or anxiety-like behaviours (OF: Supplementary Fig. S6c; EPM: Supplementary Fig. S6d) induced by CFA were greatly inhibited by ZL006. More importantly, ZL006-treated mice showed a similar data distribution as NS mice in both the OF and EPM tests (Supplementary Fig. S6c, d), unlike ibuprofen-treated mice, which

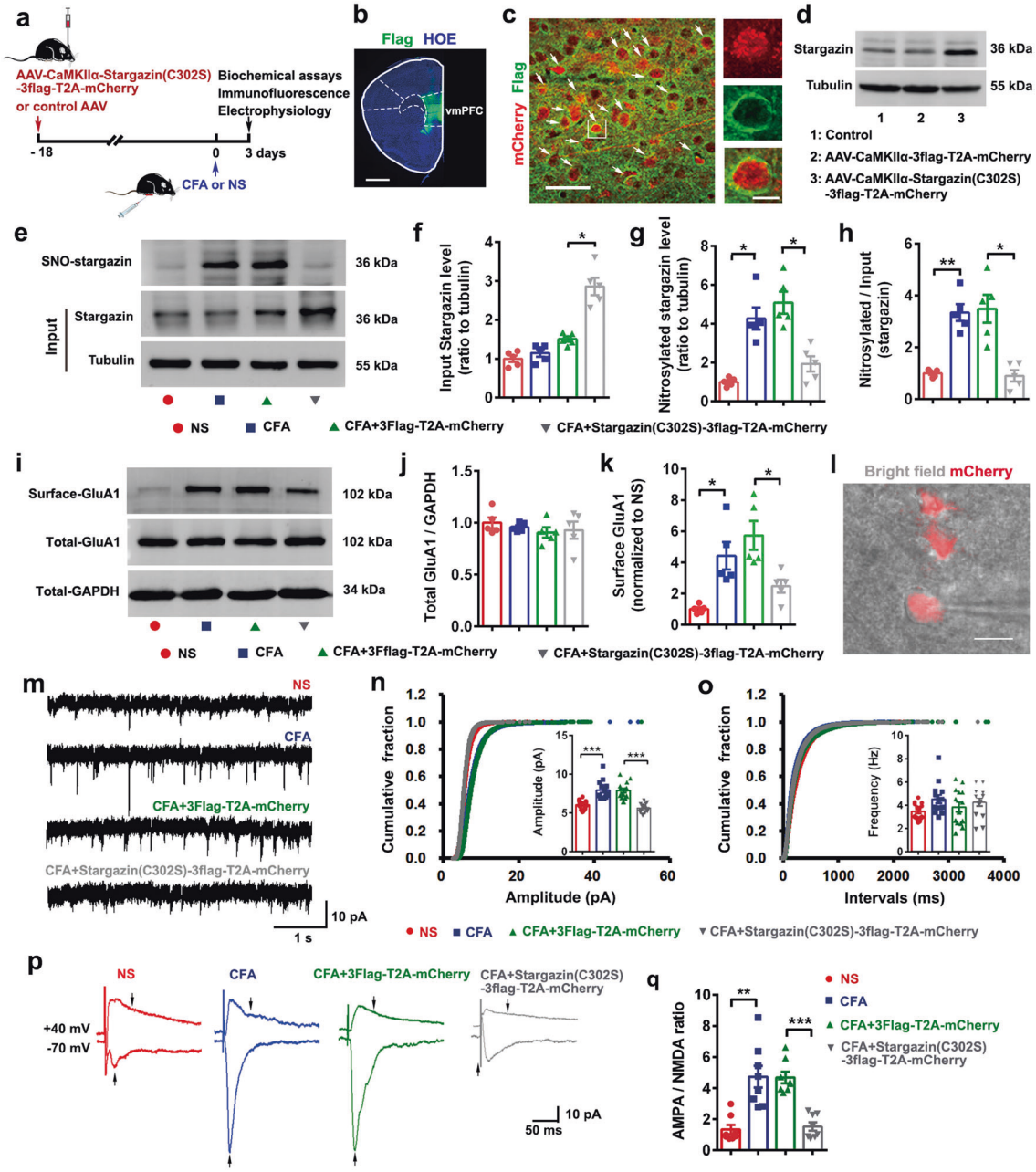

Fig. 4 The contribution of S-nitrosylated stargazin to AMPAR trafficking and function in the vmPFC. a Scheme of experimental design. **b** Coronal section showing the expression of stargazin(C302S)-3flag in the vmPFC. Similar results were observed in four mice. Scale bar, 1 mm. **c** Immunofluorescence images indicating the expression of stargazin(C302S)-3flag in the vmPFC. Arrows mark flag$^+$ cells co-labelled with mCherry$^+$ neurons. Similar results were observed in four mice. Scale bars, 50 μm (left) and 10 μm (right). **d** Representative immunoblots showing stargazin and tubulin levels in control, AAV-CaMKIIα-3flag-T2A-mCherry, and AAV-CaMKIIα-stargazin(C302S)-3flag-T2A-mCherry-infected vmPFC at Day 21 after microinjection. Representative blots of the biotin-switch assay (**e**) and dot plots showing input (**f**) and S-nitrosylated (**g**, **h**) levels of stargazin in the vmPFC. $n = 5$ for each group. Representative Western blots (**i**) and dot plots showing total (**j**) and surface (**k**) protein levels of GluA1. $n = 5$ for each group. **l** Image showing that the mCherry$^+$ pyramidal neuron on layer 2/3 in the vmPFC of AAV-infected mice was recorded for whole-cell patch-clamp 3 weeks after AAV injection. **m** Representative traces of mEPSCs. Cumulative fraction plots of mEPSC amplitude (**n**, mean amplitude in inset) and interevent intervals (**o**, mean frequency in inset). $n = 14$ neurons (from four mice) for each group. **p** Representative traces of eEPSCs in the presence of BMI (20 μM). Arrows indicate that AMPAR-EPSCs were measured at their peak at a holding potential of −70 mV, and NMDAR-EPSCs were measured 50 ms after stimulation at a holding potential of +40 mV. **q** Dot graph showing the AMPA/NMDA ratio. $n = 8$ neurons (from four mice) for each group. Data are expressed as the mean ± SEM; $^*P < 0.05$, $^{**}P < 0.01$, and $^{***}P < 0.001$ (Tukey's test following ordinary one-way ANOVA for **j**, Tamhane's T2 ($n < 50$) test following Brown-Forsythe and Welch ANOVA for **f**–**h**, **j**, **k** and Dunn's test following Kruskal–Wallis ANOVA for **n** (inset) and **o** (inset)).

displayed a high variation across the levels of the NS group and CFA group (Fig. 1c, d). These results indicated that chronic pain-induced anxiety would not persist when chronic pain was alleviated by ZL006.

DISCUSSION

In this study, we established a protocol for screening mice with persistent anxiety-like behaviours after mechanical allodynia had been attenuated by analgesic treatment and demonstrated that

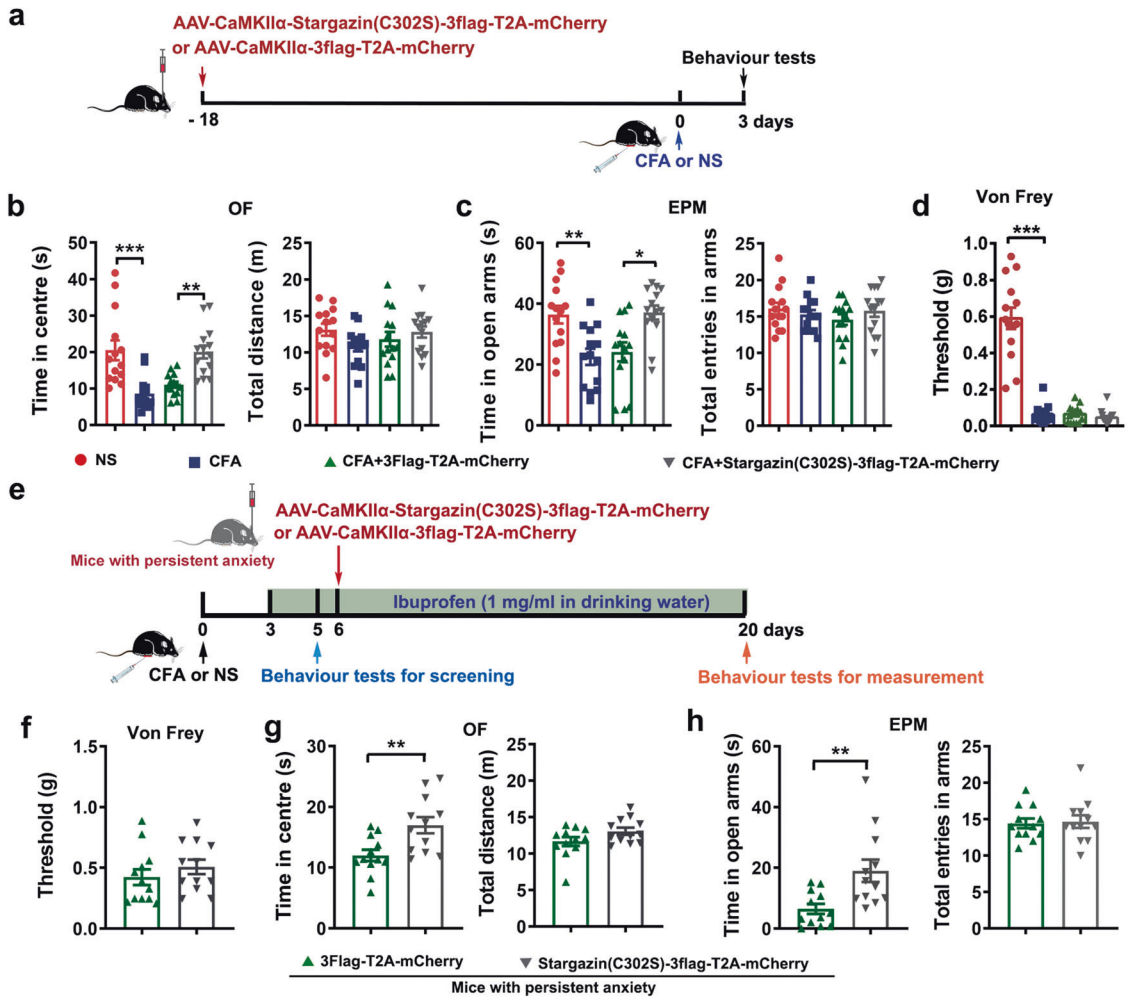

Fig. 5 Stargazin (C302S) attenuates chronic pain-induced persistent anxiety. a Experimental design for **b**–**d**. Time in centre (**b**, left) and total distance (**b**, right) in OF tests, time in open arms (**c**, left) and total entries in arms (**c**, right) in EPM tests, and withdrawal threshold of the hind paw in von Frey tests (**d**) at Day 3 after CFA or NS injection. $n = 14$ for each group. **e** Experimental design for **f**–**h**. Withdrawal threshold of the hind paw in von Frey tests (**f**), time in centre (**g**, left) and total distance (**g**, right) in OF tests, time in open arms (**h**, left) and total entries in arms (**h**, right) in EPM tests on Day 20 after CFA or NS injection. $n = 12$ for each group. Behavioural data of NS- and CFA-injected mice without ibuprofen treatment are shown in Supplementary Fig. S2. Data are the mean ± SEM; $^{*}P < 0.05$, $^{**}P < 0.01$, and $^{***}P < 0.001$ (Tukey's test following ordinary one-way ANOVA for **b** (right) and **c** (right), Tamhane's T2 test following Brown-Forsythe and Welch ANOVA for **c** (left), Dunn's test following Kruskal–Wallis ANOVA for **b** (left) and **d**, unpaired two-tailed Student's *t* test for **f**, **g** (left) and **h** (right), two-tailed Mann–Whitney *U* test for **g** (right) and two-tailed Welch's *t* test for **h** (left)).

the S-nitrosylation of stargazin in the vmPFC was necessary for AMPAR trafficking and function involved in persistent anxiety. Moreover, the nNOS-PSD-95 inhibitor ZL006 displayed anxiolytic-like effects on mice with chronic pain induced-persistent anxiety through preventing S-nitrosylation, implying that the nNOS-PSD-95 interaction is a promising therapeutic target for the clinical treatment of anxiety that is persistent even though the chronic pain has been relieved by analgesics (Fig. 9). However, it is worth noting that the above conclusion was based on CFA-induced chronic inflammatory pain and associated anxiety-like behaviours. We did not include a chronic neuropathic pain model in this study, so whether neuropathic pain-induced persistent anxiety has the same mechanism and can be attenuated by ZL006 needs further study. Moreover, our findings in the vmPFC represent integrated results from both the PL and IL. It is still undiscovered whether AMPAR trafficking in the PL or IL is responsible for the persistent anxiety-like behaviours.

Chronic pain patients have high rates of anxiety disorders [39, 40]. In the clinic, up to 40% of chronic pain patients still suffer from anxiety after using traditional analgesic therapeutics [7, 8]. Unfortunately, there is no widely recognised animal model for study in this field. The protocol established in this study for dividing analgesic-treated chronic pain mice into the anxious group and the non-anxious group is convenient for investigating chronic pain-induced persistent anxiety, which cannot be alleviated by analgesic treatment. The percentage of mice included in the anxious group of total ibuprofen-treated mice is close to the clinical data. The two standards in succession based on the average levels of normal mice in the OF and EPM tests make the screen strict, which guarantees that the included anxious mice are actually anxious and that non-anxious mice are actually not anxious, although the excluded mice may be anxious or not anxious.

AMPARs, as classic glutamate ionotropic neurotransmitter receptors, mediate the majority of fast excitatory synaptic transmission [41]. Recent studies on excitatory synaptic transmission in the anterior cingulate cortex have characterised two forms of long-term potentiation: a presynaptic form that requires kainate receptors and a postsynaptic form that requires NMDARs, which mediate the interaction between chronic pain and anxiety [38, 42].

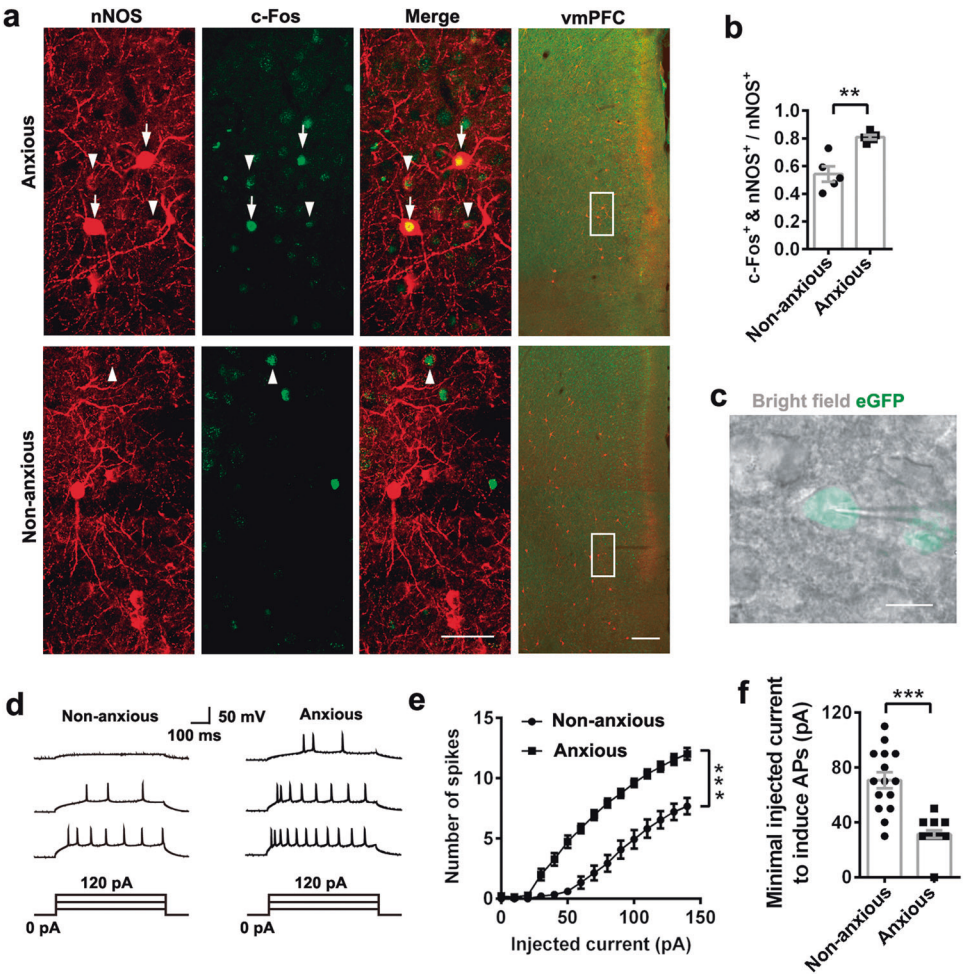

Fig. 6 Activated nNOS-expressing neurons in the vmPFC of chronic pain-induced persistent anxiety mice. Immunofluorescent images (**a**) and dot plot (**b**) showing nNOS-positive neurons colabelled with c-Fos 1 h after behavioural tests. Arrows mark type I (strongly labelled) and arrowheads mark type II (weakly labelled) nNOS-positive neurons. $n = 5$ for each group. **c** Image showing that the eGFP$^+$ pyramidal neuron on layer 2/3 in the vmPFC of AAV-hSyn-DIO-eGFP-infected nNOS-Cre mice was recorded for whole-cell current-clamp 3 weeks after AAV injection. Non-anxious and anxious mice were screened as described in Fig. 1e beginning 6 days before recordings. Scale bar, 50 μm (left) and 200 μm (right). Representative APs traces (**d**) and number of APs (**e**) evoked by various current steps (from 0 to 140 pA in 10 pA steps). $n = 15$ (from four mice) for each group. **f** Dot plot showing the minimal injected current to induce APs. $n = 15$ (from four mice) for each group. Data are the mean ± SEM; $^{**}P < 0.01$ and $^{***}P < 0.001$ (two-tailed Welch's t test for b, two-tailed Mann–Whitney U test for **f** and two-way ANOVA for **e**).

Furthermore, administration of the AMPAR antagonist CNQX to the infralimbic cortex induces anxiolytic-like effects [14]. Membrane AMPAR subunit GluA1 overexpression occurs as a result of nerve injury [43]. Regulation of AMPAR membrane trafficking is critical for synaptic plasticity in the brain, which contributes to many neuropsychiatric diseases. Our results in this study establish the importance of AMPAR trafficking and AMPAR-dependent synaptic transmission in the vmPFC for chronic pain-induced anxiety, especially persistent anxiety after chronic pain has been alleviated by analgesic treatment, and are consistent with pharmacological studies with AMPAR agonists and antagonists [14, 44]. In addition to AMPARs, NMDARs also contribute to synaptic glutamatergic neurotransmission meditating anxiety and pain. Local microinjection of an NMDA receptor antagonist, MK-801, in the prelimbic medial prefrontal cortex completely diminished anxiety-like behaviours [15]; the partial sciatic nerve ligation model of neuropathic pain in rats can alter the expression of NMDAR subunits GluN1 and GluN2B in the hippocampus [45]. NMDAR transmission mediates NO diffusion by nNOS activation [46], which, in turn, impacts AMPAR trafficking [47]. Moreover, the nNOS-PSD-95 interaction is related to NMDAR activation [24]. Thus, there is crosstalk between AMPARs and NMDARs for chronic pain induced anxiety. Here, we verified that the nNOS-PSD-95 inhibitor ZL006 reversed the persistent anxiety-like behaviours of mice that could not be relieved by regular analgesics. This is a therapeutic strategy connecting AMPARs and NMDARs. On the other hand, the details of how these two glutamate receptors work in coordination with each other in the regulation of chronic pain-induced persistent anxiety remain unknown, and more attention should be given to looking for novel drug targets in further studies.

S-nitrosylation, phosphorylation, and palmitoylation occurring in the brain mediate AMPAR trafficking [22, 23, 48–50], and the crucial role of S-nitrosylation has been well established in several studies. The findings of Selvakumar et al. showed that S-nitrosylation of the AMPAR subunit GluA1 regulates the surface expression and function of AMPARs [49]. Moreover, S-nitrosylation of AMPAR-interacting proteins, such as stargazin, 4.1 N protein, and NeSF, also contributes to AMPAR trafficking [22, 23]. Our results revealed that an enhanced level of stargazin S-nitrosylation mediated AMPAR trafficking in the vmPFC under chronic pain-induced anxiety conditions. However, we cannot exclude the contributions of S-nitrosylation of AMPAR subunits themselves and other AMPAR-interacting proteins in chronic pain-induced

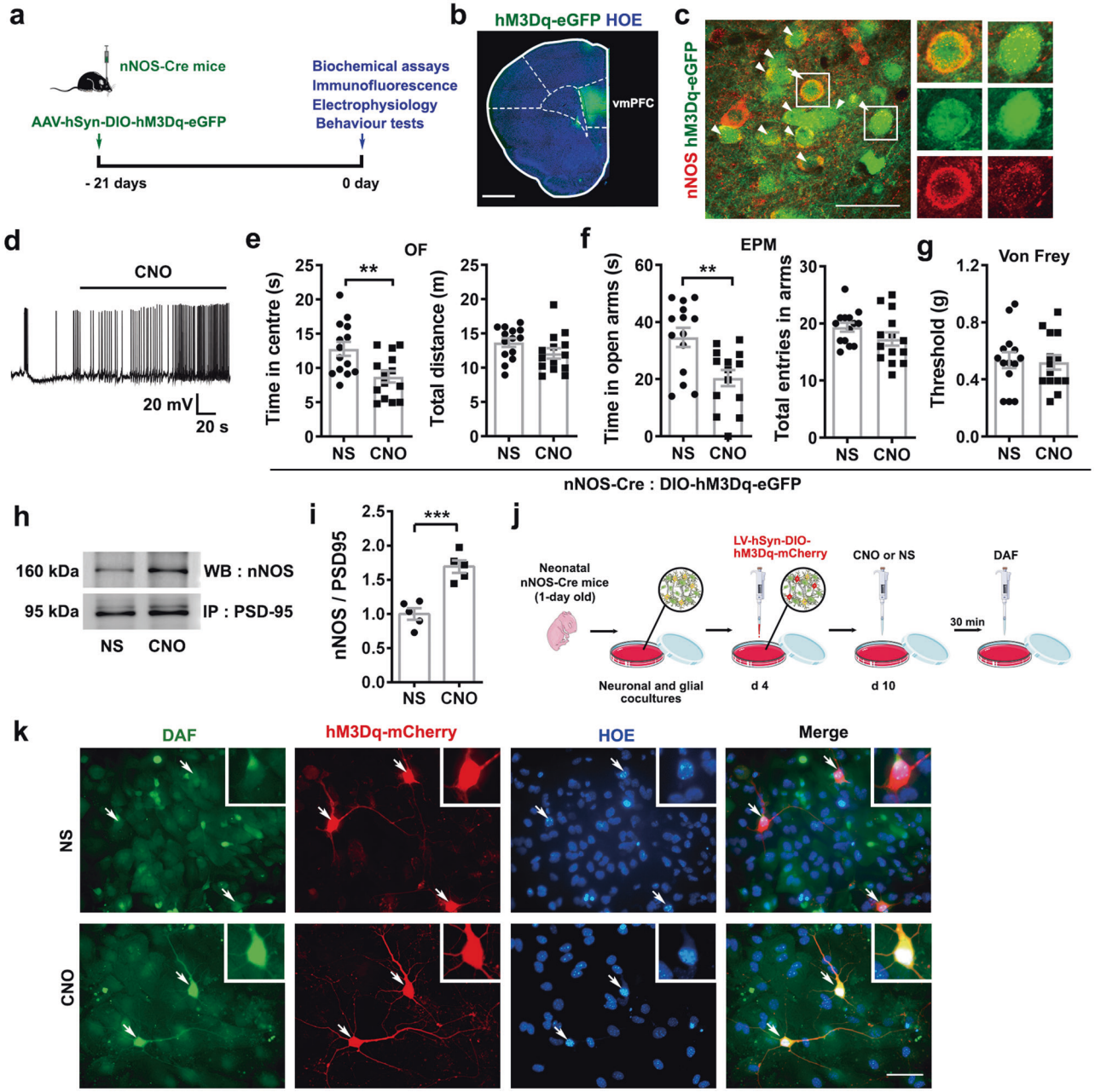

Fig. 7 Chemogenetic excitation of nNOS-expressing neurons induced nNOS-PSD-95 coupling, NO production and anxiety-like behaviours. a Scheme of experimental design. **b** Coronal section showing the expression of hM3Dq-eGFP in the vmPFC of nNOS-Cre mice. Similar results were observed in three mice. Scale bar, 1 mm. **c** Immunofluorescent images indicating the expression of hM3Dq-eGFP in vmPFC nNOS-expressing neurons. Arrows mark type I (strongly labelled) and arrowheads mark type II (weakly labelled) nNOS-positive neurons. Similar results were observed in three mice. Scale bar, 50 μm. **d** Bath application of CNO (5 μM) elicited action potential firing in neurons expressing hM3Dq-eGFP in brain slices of nNOS-Cre mice. Similar results were recorded in four neurons from two mice. Time in the centre (**e**, left) and total distance (**e**, right) in the OF tests, time in the open arms (**f**, left) and total entries in the arms (**f**, right) in the EPM tests, and withdrawal threshold of the hind paw in the von Frey tests (**g**) 21 days after AAV-hSyn-DIO-hM3Dq-eGFP microinjection. $n = 14$ for each group. **h**, **i** Co-IP showing PSD-95-nNOS complex levels in the vmPFC of mice 30 min after CNO (2 mg/kg, ip.) or NS treatment after AAV microinjection. $n = 5$ for each group. **j** Experimental design for **k**. Cocultures were infected with LV-hSyn-DIO-hM3Dq-mCherry at day 4 in vitro, and CNO (10 μM) was applied at day 10 in vitro to specifically activate nNOS neurons in cocultures through Cre-dependent hM3Dq expression. **k** Images showing NO levels in living nNOS-expressing neurons (mCherry$^+$) after 60 min of incubation with 20 μM DAF-FM DA. Similar results were observed in three independent experiments. Scale bar, 50 μm. WB, Western blot; IP, Immunoprecipitation. Data are the mean ± SEM; $^{**}P < 0.01$, $^{***}P < 0.001$ (unpaired two-tailed Student's *t* test for **e**–**g**, **i**).

anxiety, since NO derived from nNOS-expressing neurons is not specific for stargazin. We also found that the S-nitrosylation level of NeSF was increased in mice with chronic pain-induced persistent anxiety. Why could the anxiety-like behaviours be completely rescued with stargazin(C302S)-expressing AAV? The unique structure and function of stargazin as a member of the transmembrane AMPAR regulatory protein family provide an answer. Stargazin is a small tetraspanning membrane protein and interacts with most AMPAR subunits, especially GluA1 [22], and GluA1 and GluA2 subunits are expressed in the majority of AMPA

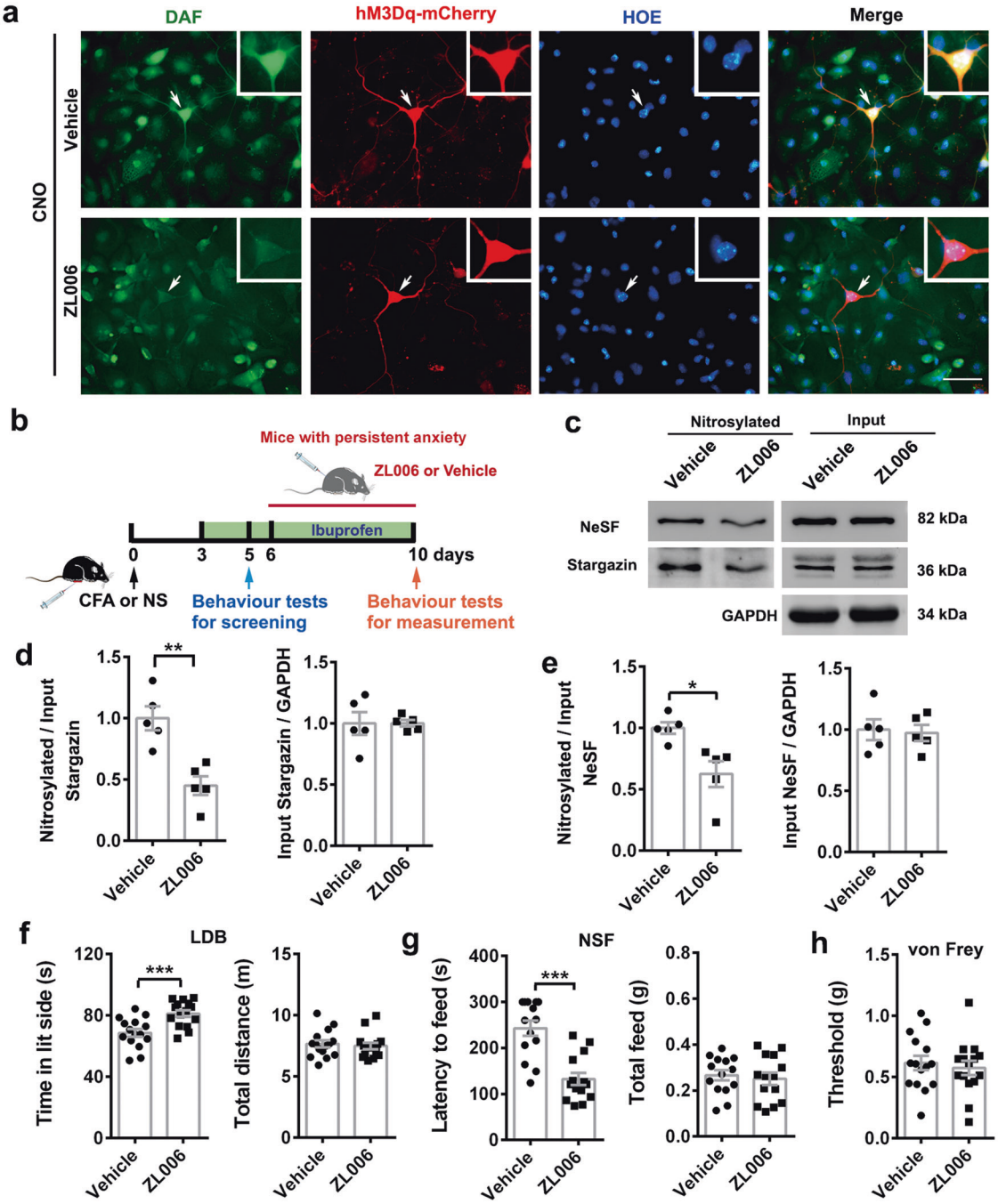

Fig. 8 ZL006 attenuates chronic pain-induced persistent anxiety. a Images showing NO levels in living nNOS-expressing neurons (mCherry^{+}) after 60 min of incubation with 20 μM DAF-FM DA. The protocol was the same as that shown in Fig. 7j, except that ZL006 (10 μM) or vehicle was added along with CNO. Similar results were observed in 3 independent experiments. Scale bar, 50 μm. **b** Experimental design for **c**–**h.** Representative blots of the biotin-switch assay (**c**) and dot plots showing S-nitrosylation and input levels of stargazin (**d**) and NeSF (**e**) in the vmPFC. $n = 5$ for each group. Time in side with light (**f**, left) and total distance (**f**, right) in LDB tests, latency to feed (**g**, left) and total feed (**g**, right) in NSF tests and withdrawal threshold of hind paw in von Frey tests (**h**) after continuous 5-day administration of ZL006 (20 mg/kg, ip., once a day). Behavioural tests were performed 30 min after the last ZL006 administration. $n = 15$ for each group in LDB and von Frey tests, $n = 14$ for each group in NSF tests (one mouse in each group was excluded from analysis for accidental noise during the test). Behavioural data of NS- and CFA-injected mice without ibuprofen treatment are shown in Supplementary Fig. S5. Data are the mean ± SEM; $^{*}P < 0.05$, $^{**}P < 0.01$, and $^{***}P < 0.001$ (unpaired two-tailed Student's *t* test for **d** (left), **e**, **f** (left), **g** (right) and **h**, two-tailed Welch's *t* test for **d** (right) and two-tailed Mann–Whitney *U* test for **f** (right) and **g** (left)).

receptors in the nervous system [51, 52]; thus, stargazin is a principal regulator of AMPAR membrane expression. Moreover, deficiency in any factor involved in AMPAR membrane trafficking would damage the eventual synaptic transmission, since AMPARs are tetrameric assemblies of homologous subunits encoded by four different genes (GluA1-4), which combine in different stoichiometries to form functional receptor subtypes [17].

Although S-nitrosylated stargazin is essential to chronic pain-induced persistent anxiety, it is difficult to inhibit S-nitrosylation by targeting stargazin itself with small molecular compounds.

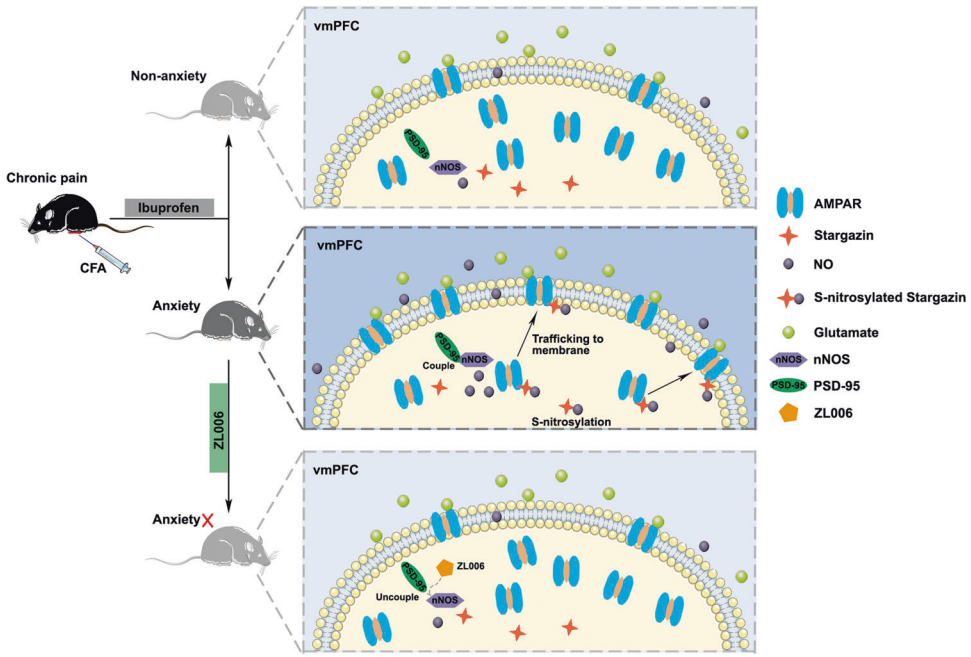

Fig. 9 Summary model diagram. AMPAR trafficking by S-nitrosylation is enhanced in the vmPFC of mice with persistent anxiety following chronic inflammatory pain, and ZL006 rescues chronic inflammatory pain-induced persistent anxiety.

We have demonstrated that vmPFC nNOS-expressing neurons are critical to transform chronic pain signals into anxiety-like behaviours in mice [12] and further confirmed their role in persistent anxiety even though chronic pain was relieved by analgesics in this study. NO production after enhanced interaction of nNOS with PSD-95 in activated vmPFC nNOS-expressing neurons is responsible for S-nitrosylation of stargazin, so nNOS-PSD-95 interaction inhibitor would be a good choice for indirect downregulation of S-nitrosylated stargazin. Fortunately, animal behavioural experiments with ZL006 verified our speculation. ZL006 is a small molecular inhibitor of the nNOS-PSD-95 interaction, which was initially designed and synthesised in our laboratory to prevent neuronal excitotoxicity after acute cerebral ischaemia [24]. Recently, we and other researchers discovered that ZL006 is effective in diverse preclinical models of chronic pain [30, 53–55]. The results from this study demonstrated that ZL006 could alleviate chronic pain-induced persistent anxiety in mice, indicating that the nNOS-PSD-95 interaction is a promising therapeutic target for the clinical treatment of anxiety that cannot be relieved by regular analgesics. More importantly, targeting the nNOS-PSD-95 interaction showed the potential to treat both chronic pain and comorbid anxiety simultaneously, implying a possible advantage over regular analgesics.

ACKNOWLEDGEMENTS

This work was supported by grants from the National Brain Research Programme of China (2022ZD0211703), National Natural Science Foundation of China (82171293, 82090042), Natural Science Foundation of Jiangsu Province (BK20211255), Fujian Province Natural Science Foundation (2021J011433), and Fujian Provincial Health Technology Project (2021QNA072). The authors thank D. Yang and J.T. Wang for technical assistance with the behavioural tests.

AUTHOR CONTRIBUTIONS

ZJC, CWS, SX and TL carried out and analysed the behavioural tests. ZJC, CWS, SX and HYL performed and analysed the electrophysiological experiments, fluorescent imaging experiments, and biochemical assays. LC and HYW prepared chronic pain models and conducted cannulations and microinjections. YHL directed the electrophysiological experiments. FL synthesised ZL006. CXL and DYZ conceived the study. ZJC wrote the first draft of the paper. CXL designed and directed the experiments and wrote the paper.

ADDITIONAL INFORMATION

Supplementary information The online version contains supplementary material available at https://doi.org/10.1038/s41401-022-01024-z.

Competing interests: The authors declare no competing interests.

REFERENCES

1. Dersh J, Polatin PB, Gatchel RJ. Chronic pain and psychopathology: research findings and theoretical considerations. Psychosom Med. 2002;64:773–86.
2. Price DD. Psychological and neural mechanisms of the affective dimension of pain. Science. 2000;288:1769–72.
3. Velly AM, Mohit S. Epidemiology of pain and relation to psychiatric disorders. Prog Neuropsychopharmacol Biol Psychiatry. 2018;87:159–67.
4. Bair MJ, Wu J, Damush TM, Sutherland JM, Kroenke K. Association of depression and anxiety alone and in combination with chronic musculoskeletal pain in primary care patients. Psychosom Med. 2008;70:890–7.
5. Bruffaerts R, Demyttenaere K, Kessler RC, Tachimori H, Bunting B, Hu C, et al. The associations between preexisting mental disorders and subsequent onset of chronic headaches: a worldwide epidemiologic perspective. J Pain. 2015;16:42–52.
6. de Heer EW, Gerrits MM, Beekman AT, Dekker J, van Marwijk HW, de Waal MW, et al. The association of depression and anxiety with pain: a study from NESDA. PLoS One. 2014;9:e106907.
7. Feingold D, Brill S, Goor-Aryeh I, Delayahu Y, Lev-Ran S. Depression and anxiety among chronic pain patients receiving prescription opioids and medical marijuana. J Affect Disord. 2017;218:1–7.
8. Hasanpour-Dehkordi A, Solati K, Tali SS, Dayani MA. Effect of progressive muscle relaxation with analgesic on anxiety status and pain in surgical patients. Br J Nurs. 2019;28:174–8.
9. Myers-Schulz B, Koenigs M. Functional anatomy of ventromedial prefrontal cortex: implications for mood and anxiety disorders. Mol Psychiatry. 2012;17:132–41.
10. Zhuo M. Neural mechanisms underlying anxiety-chronic pain interactions. Trends Neurosci. 2016;39:136–45.
11. Wang GQ, Cen C, Li C, Cao S, Wang N, Zhou Z, et al. Deactivation of excitatory neurons in the prelimbic cortex via Cdk5 promotes pain sensation and anxiety. Nat Commun. 2015;6:7660.
12. Liang HY, Chen ZJ, Xiao H, Lin YH, Hu YY, Chang L, et al. nNOS-expressing neurons in the vmPFC transform pPVT-derived chronic pain signals into anxiety behaviors. Nat Commun. 2020;11:2501.
13. Hung KL, Wang SJ, Wang YC, Chiang TR, Wang CC. Upregulation of presynaptic proteins and protein kinases associated with enhanced glutamate release from axonal terminals (synaptosomes) of the medial prefrontal cortex in rats with neuropathic pain. Pain. 2014;155:377–87.

14. Bi LL, Wang J, Luo ZY, Chen SP, Geng F, Chen YH, et al. Enhanced excitability in the infralimbic cortex produces anxiety-like behaviors. Neuropharmacology. 2013;72:148–56.
15. Saitoh A, Ohashi M, Suzuki S, Tsukagoshi M, Sugiyama A, Yamada M, et al. Activation of the prelimbic medial prefrontal cortex induces anxiety-like behaviors via N-Methyl-D-aspartate receptor-mediated glutamatergic neurotransmission in mice. J Neurosci Res. 2014;92:1044–53.
16. Kerchner GA, Nicoll RA. Silent synapses and the emergence of a postsynaptic mechanism for LTP. Nat Rev Neurosci. 2008;9:813–25.
17. Traynelis SF, Wollmuth LP, McBain CJ, Menniti FS, Vance KM, Ogden KK, et al. Glutamate receptor ion channels: structure, regulation, and function. Pharmacol Rev. 2010;62:405–96.
18. Wenthold RJ, Petralia Rs Fau - Blahos J Ii, Blahos J, Ii Fau - Niedzielski AS, Niedzielski AS. Evidence for multiple AMPA receptor complexes in hippocampal CA1/CA2 neurons. J Neurosci. 1996;16:1982–9.
19. O'Brien RJ, Kamboj S, Ehlers MD, Rosen KR, Fischbach GD, Huganir RL. Activity-dependent modulation of synaptic AMPA receptor accumulation. Neuron. 1998;21:1067–78.
20. Penn AC, Zhang CL, Georges F, Royer L, Breillat C, Hosy E, et al. Hippocampal LTP and contextual learning require surface diffusion of AMPA receptors. Nature. 2017;549:384–8.
21. Lissin DV, Gomperts SN, Carroll RC, Christine CW, Kalman D, Kitamura M, et al. Activity differentially regulates the surface expression of synaptic AMPA and NMDA glutamate receptors. Proc Natl Acad Sci USA. 1998;95:7097–102.
22. Selvakumar B, Huganir RL, Snyder SH. S-nitrosylation of stargazin regulates surface expression of AMPA-glutamate neurotransmitter receptors. Proc Natl Acad Sci USA. 2009;106:16440–5.
23. Huang Y, Man HY, Sekine-Aizawa Y, Han Y, Juluri K, Luo H, et al. S-nitrosylation of N-ethylmaleimide sensitive factor mediates surface expression of AMPA receptors. Neuron. 2005;46:533–40.
24. Zhou L, Li F, Xu HB, Luo CX, Wu HY, Zhu MM, et al. Treatment of cerebral ischemia by disrupting ischemia-induced interaction of nNOS with PSD-95. Nat Med. 2010;16:1439–43.
25. Percie du Sert N, Hurst V, Ahluwalia A, Alam S, Avey MT, Baker M, et al. The ARRIVE guidelines 2.0: Updated guidelines for reporting animal research. PLoS Biol. 2020;18:e3000410.
26. Jiang J, Shen YY, Li J, Lin YH, Luo CX, Zhu DY. (+)-Borneol alleviates mechanical hyperalgesia in models of chronic inflammatory and neuropathic pain in mice. Eur J Pharmacol. 2015;757:53–8.
27. Zhu LJ, Li TY, Luo CX, Jiang N, Chang L, Lin YH, et al. CAPON-nNOS coupling can serve as a target for developing new anxiolytics. Nat Med. 2014;20:1050–4.
28. Warner-Schmidt JL, Vanover KE, Chen EY, Marshall JJ, Greengard P. Antidepressant effects of selective serotonin reuptake inhibitors (SSRIs) are attenuated by antiinflammatory drugs in mice and humans. Proc Natl Acad Sci USA. 2011;108:9262–7.
29. Ma L, Yue L, Zhang Y, Wang Y, Han B, Cui S, et al. Spontaneous pain disrupts ventral hippocampal CA1-infralimbic cortex connectivity and modulates pain progression in rats with peripheral inflammation. Cell Rep. 2019;29:1579–93.
30. Li J, Zhang L, Xu C, Shen YY, Lin YH, Zhang Y, et al. A pain killer without analgesic tolerance designed by co-targeting PSD-95-nNOS interaction and alpha2-containning GABAARs. Theranostics. 2021;11:5970–85.
31. Yin CY, Huang SY, Gao L, Lin YH, Chang L, Wu HY, et al. Neuronal nitric oxide synthase in nucleus accumbens specifically mediates susceptibility to social defeat stress through cyclin-dependent kinase 5. J Neurosci. 2021;41:2523–39.
32. Luo CX, Zhu XJ, Zhou QG, Wang B, Wang W, Cai HH, et al. Reduced neuronal nitric oxide synthase is involved in ischemia-induced hippocampal neurogenesis by up-regulating inducible nitric oxide synthase expression. J Neurochem. 2007;103:1872–82.
33. Lin Y, Yao M, Wu H, Wu F, Cao S, Ni H, et al. Environmental enrichment implies GAT-1 as a potential therapeutic target for stroke recovery. Theranostics. 2021;11:3760–80.
34. Luo CX, Lin YH, Qian XD, Tang Y, Zhou HH, Jin X, et al. Interaction of nNOS with PSD-95 negatively controls regenerative repair after stroke. J Neurosci. 2014;34:13535–48.
35. Lin YH, Liang HY, Xu K, Ni HY, Dong J, Xiao H, et al. Dissociation of nNOS from PSD-95 promotes functional recovery after cerebral ischaemia in mice through reducing excessive tonic GABA release from reactive astrocytes. J Pathol. 2018;244:176–88.
36. Ferreira AN, Yousuf H, Dalton S, Sheets PL. Highly differentiated cellular and circuit properties of infralimbic pyramidal neurons projecting to the periaqueductal gray and amygdala. Front Cell Neurosci. 2015;9:161.
37. Li K, Nakajima M, Ibañez-Tallon I, Heintz N. A cortical circuit for sexually dimorphic oxytocin-dependent anxiety behaviors. Cell. 2016;167:60–72.e11.
38. Koga K, Descalzi G, Chen T, Ko HG, Lu J, Li S, et al. Coexistence of two forms of LTP in ACC provides a synaptic mechanism for the interactions between anxiety and chronic pain. Neuron. 2015;85:377–89.
39. Demyttenaere K, Bruffaerts R, Lee S, Posada-Villa J, Kovess V, Angermeyer MC, et al. Mental disorders among persons with chronic back or neck pain: results from the World Mental Health Surveys. Pain. 2007;129:332–42.
40. Gerrits M, Vogelzangs N, van Oppen P, van Marwijk HWJ, van der Horst H, Penninx B. Impact of pain on the course of depressive and anxiety disorders. Pain. 2012;153:429–36.
41. Song I, Huganir RL. Regulation of AMPA receptors during synaptic plasticity. Trends Neurosci. 2002;25:578–88.
42. Bliss TV, Collingridge GL, Kaang BK, Zhuo M. Synaptic plasticity in the anterior cingulate cortex in acute and chronic pain. Nat Rev Neurosci. 2016;17:485–96.
43. Xu H, Wu LJ, Wang H, Zhang X, Vadakkan KI, Kim SS, et al. Presynaptic and postsynaptic amplifications of neuropathic pain in the anterior cingulate cortex. J Neurosci. 2008;28:7445–53.
44. Solati J, Hajikhani R, Golub Y. Activation of GABAA receptors in the medial prefrontal cortex produces an anxiolytic-like response. Acta Neuropsychiatr. 2013;25:221–6.
45. Wang XQ, Zhong XL, Li ZB, Wang HT, Zhang J, Li F, et al. Differential roles of hippocampal glutamatergic receptors in neuropathic anxiety-like behavior after partial sciatic nerve ligation in rats. BMC Neurosci. 2015;16:14.
46. Bredt DS, Snyder SH. Nitric oxide mediates glutamate-linked enhancement of cGMP levels in the cerebellum. Proc Natl Acad Sci USA. 1989;86:9030–3.
47. Shi SH, Hayashi Y, Petralia RS, Zaman SH, Wenthold RJ, Svoboda K, et al. Rapid spine delivery and redistribution of AMPA receptors after synaptic NMDA receptor activation. Science. 1999;284:1811–6.
48. Lee HK, Takamiya K, Han JS, Man H, Kim CH, Rumbaugh G, et al. Phosphorylation of the AMPA receptor GluR1 subunit is required for synaptic plasticity and retention of spatial memory. Cell. 2003;112:631–43.
49. Selvakumar B, Jenkins MA, Hussain NK, Huganir RL, Traynelis SF, Snyder SH. S-nitrosylation of AMPA receptor GluA1 regulates phosphorylation, single-channel conductance, and endocytosis. Proc Natl Acad Sci USA. 2013;110:1077–82.
50. Lu W, Roche KW. Posttranslational regulation of AMPA receptor trafficking and function. Curr Opin Neurobiol. 2012;22:470–9.
51. Reimers JM, Milovanovic M, Wolf ME. Quantitative analysis of AMPA receptor subunit composition in addiction-related brain regions. Brain Res. 2011;1367:223–33.
52. Schwenk J, Baehrens D, Haupt A, Bildl W, Boudkkazi S, Roeper J, et al. Regional diversity and developmental dynamics of the AMPA-receptor proteome in the mammalian brain. Neuron. 2014;84:41–54.
53. Lee WH, Xu Z, Ashpole NM, Hudmon A, Kulkarni PM, Thakur GA, et al. Small molecule inhibitors of PSD95-nNOS protein-protein interactions as novel analgesics. Neuropharmacology. 2015;97:464–75.
54. Cai W, Wu S, Pan Z, Xiao J, Li F, Cao J, et al. Disrupting interaction of PSD-95 with nNOS attenuates hemorrhage-induced thalamic pain. Neuropharmacology. 2018;141:238–48.
55. Carey LM, Lee WH, Gutierrez T, Kulkarni PM, Thakur GA, Lai YY, et al. Small molecule inhibitors of PSD95-nNOS protein-protein interactions suppress formalin-evoked Fos protein expression and nociceptive behavior in rats. Neuroscience. 2017;349:303–17.

Springer Nature or its licensor (e.g. a society or other partner) holds exclusive rights to this article under a publishing agreement with the author(s) or other rightsholder(s); author self-archiving of the accepted manuscript version of this article is solely governed by the terms of such publishing agreement and applicable law.